Biochar for adsorption remediation of Ciprofloxacin in wastewater

Supervisor: Sachin Maruti Chavan

Author: Bilal Asghar

Department of Chemistry, Bioscience and Environmental Engineering.

University of Stavanger

Abstract

Ciprofloxacin is one of the major pharmaceutical pollutants being fed into waterbodies around the world. It is consumed by humans and animals, passed into the environment mainly through hospital waste. Ciprofloxacin, an antibiotic could be very harmful for environmental, disturbing the natural balance and can further increase the problem of antibiotic resistance. This thesis aims to study biochar as an adsorbent to remove ciprofloxacin from wastewater. Nine samples of biochar from wood and sludge pyrolyzed at different temperatures were characterized using XRD, FTIR, TGA and BET using Nitrogen and Carbon dioxide. Finally, batch equilibrium method was performed to investigate the sorption of ciprofloxacin on biochar. The results showed overall promising protentional of biochar for sorption of Ciprofloxacin. Wood biochar pyrolyzed at higher temperature exhibited larger specific area and more micropore volume as compared to sludge samples of same temperature, hence better suited for the task. In batch adsorption, wood and sludge sample did not reach saturation point and showed lower sorption capacity from literature. Also, the sorption capacity trend which was expected to increase did not match with previous data for sludge sample. This could be due to lower adsorbent quantity and Ciprofloxacin concentration used and variation in biochar composition especially sludge. Future study with changing suggested variables like mass of biochar, concentration of Ciprofloxacin, and changing temperature etc will help fully understand its sorption capacity and eventually support in application of biochar in adsorption of ciprofloxacin.

1 Table of Contents

1 Table of Contents 3
List of Abbreviations: 5
List of Figures 6
List of Tables 8
1. Introduction 9
1.1. Challenges of pharmaceuticals in environment 10
1.2. Effects on environment 11
2. Literature review 14
2.1. Adsorption for removal of CIP 14
2.2. Biochar as an adsorbent 15
3. Problem statement of the thesis: 18
2 Materials and methods 19
2.1 Materials 19
Methods 20
2.1.1 Characterization Techniques 20
2.2 XRD 21
2.3 ATR-FTIR 23
2.4 TGA 24
2.5 BET 25
2.6 Nitrogen Sorption 27
2.7 Carbon dioxide sorption 27
2.8 Ultraviolet-visible (UV) spectroscopy 28
2.9 Batch adsorption 30
2.10 Sorption isotherm analysis: 33
3 Results and Discussion 34
3.1 XRD analysis 34
3.2 FT-IR (ATR) 38
3.3 TGA 42
3.4 BET: 48

3.4.1 Pore size distribution: 53
3.4.2 CO_2 adsorption 55
3.4.3 Drug-uptake 56
3.4.4 Ciprofloxacin and Sludge biochar: 61
3.4.5 Ciprofloxacin and wood biochar: 64
4 Conclusion 68
5 References 69

List of Abbreviations:

AC	Carbon
BET	Brunauer–Emmett–Teller
BJH	Barrett - Joyner - Halenda. Analysis of pore distribution
CIP	Ciprofloxacin
DNA	Deoxyribonucleic acid
FTIR	Attenuated total reflectance-Fourier transform infrared
FQ	Fluoroquinolone
IUPAC	International Union of Pure and Applied Chemistry
TA	Thermal analysis
TGA	Thermogravimetric Analysis
XRD	X-ray Diffraction
UV	Ultraviolet
WWTP	Wastewater treatment plant

List of Figures

Figure 1. Global pharmaceutical detection of substances in drinking waters, groundwater, and surface waters. [1] ..... **Error! Bookmark not defined.**
Figure 2 Structure of Ciprofloxacin [4] 14
Figure 3Schematic diagram of XRD from crystal planes 22
Figure 4 Schematic representation of FT-IR 24
Figure 5 . The IUPAC Classifications of Gas-Solid Equilibria Adsorption Isotherm models 26
Figure 6 . Schematic representation of UV spectroscopy 28
Figure 7. Laboratory picture CIP solution 30
Figure 8 a) IKA Ms 3 basics. B) Batch sorption setup 31
Figure 9 XRD spectra of Biochar obtained from wood at various pyrolysis temperatures 35
Figure 10 XRD spectrum of biochar obtained from sewage sludge at 500°C, 600°C, 700°C, 800°C and 15% moisture 37
Figure 11 FTIR analysis of biochar obtained from wood at various pyrolysis temperatures 38
figure 12 : FT-IR spectra of biochar derived from sludge at various pyrolysis temperatures. 40
Figure 13 TGA of wood biochar samples at various temperatures under inert atmosphere with N2-flow of 25mL/min 42
Figure 14 weight loss measurement of wood biochar samples under synthetic air flow (25 mL/min) at 900 °C 44
Figure 15 TGA of sludge biochar samples at various temperatures under inert atmosphere with N2-flow 45
Figure 16 . Weight loss% of sludge biochar samples under synthetic air flow (25 mL/min) at 900°C 47
Figure 17 BET-measurement of biochar-wood samples 49
Figure 18 BET-measurement of biochar-wood samples 51
Figure 19Pore distribution BJH for wood samples at 550oc, 600oC, and 750oC 53
Figure 20. Pore distribution BJH for sludge samples at 550oc, 600oC, 700oC, 800oC, and 15% moisture 53
Figure 21 CO2 adsorption isotherms of wood samples 55
Figure 22 CO2 adsorption isotherms of sludge samples 55
Figure 23 UV spectra of ciprofloxacin using different concentrations (1 – 6 mg/L) 56
figure 24 Calibration curve of ciprofloxacin 57
Figure 25 UV spectra of 1mg/L, thrice spectra measurement 58
Figure 26 UV spectra of 3 different samples of 6mg/L spectra 59
Figure 27 Adsorption isotherm models of ciprofloxacin on the sludge biochar samples 61
Figure 28 Langmuir and Freundlich models for sludge samples plotted from equation 7 and equation 8 63

Figure 29 . Adsorption isotherm models of ciprofloxacin on the wood biochar samples..... 64
Figure 30 UV spectra for wood sample 700C ..... **Error! Bookmark not defined.**
Figure 31 Langmuir and Freundlich linear isotherm plot for WPB-550 and WPB-600 plotted from equation 7 and equation 8..... 65
Figure 32 Langmuir and Freundlich linear isotherm plot for WPB-550 and WPB-600..... 66

List of Tables

Table 1Effects of pharmaceuticals on non-target organisms (Patel et al, 2019) 13
Table 2: Conventional treatment processes for pharmaceuticals (Patel et al, 2019) 17
Table 3 Samples of biochar adsorbent obtained from wood and sludge at different pyrolysis temperature 19
Table 4 Chemical composition of the wood biochar samples pyrolyzed at elevated temperatures 43
Table 5 : Chemical composition of the wood biochar samples pyrolyzed at elevated temperatures 46
Table 6 Surface area. Monolayer volume and total pore volume of wood samples 50
Table 7 Surface area. Monolayer volume and total pore volume of sludge samples 52
Table 8 Standard deviation measurements in 3 samples of 1mg/L solutions 58
Table 9 standard deviation measurements in 3 samples of 6mg/L solutions 60

1. Introduction

Since the advent of modern science and big pharma, usage of pharmaceutical drugs has increased many folds, as it has helped save millions of lives but now it has a contributed a significant share in contamination of environment. In more recent year's studies have found out presence of these contaminants in rivers, lakes to seawater and from effluents of wastewater treatment plants (WWTP).

Especially in last three decades, pharmaceutical wastes residue has been traced in almost in every continent even unpopulated North and South polar region have not been spared where numerous endocrine disruptors, synthetic oestrogen and caffeine have been found. According to German environmental agency, which reviewed data from 71 countries, found out that pharmaceutical contaminants are widely distributed, degrading at different rates lead from complete degradation to partial degradation in the natural environment and WWTPs. Pharmaceuticals mostly are not highly non-biodegradable but continuous addition into the environment even in small amounts can make it "pseudo-persistent".

Normally WWTP are not designed to treat this class of environmental contaminants, but many methods can be used in treatment of pharmaceuticals in wastewater like photolysis, degradation, oxidation, usage of membrane technology, specifically nano filtration, reverse osmosis, and adsorption. There are many drawbacks to these methods that cause limitations in application of these methods like generation of toxic sludge, limited removal, high costs rendering the process uneconomical, and requirement for trained worker for operations and maintenance tasks (Patel et al., 2019). Adsorption with biochar is a relatively low-cost method that could be applicable in developing countries where normally high costs and limited technology is a grave issue, also adsorption methods could be easily integrated in conventional and modern wastewater treatments plants.

1.1. Challenges of pharmaceuticals in environment

After discovery of first ever active pharmaceutical discovered in water in 1980s, there have been a range of types of compounds found and studied. According to Bush, these compounds can be grouped as:

1. Analgesics or Anti-inflammatory drugs e.g., ibuprofen and paracetamol
2. Antibiotics e.g., Ciprofloxacin, Penicillin
3. Antiepileptics
4. Antidepressants
5. Fibrates
6. Antihistamines/anti allergenics (famotidine, ranitidine)
7. β-blockers (propranolol)
8. Other compounds like antiseptics and narcotics

Antibiotics have been found to be most abundantly occurring followed by analgesics. But these results vary depending on manufacturing units' locations, countries, regions, socio-economical and seasonal factors. Scientists believe that the data of geographical distribution is not enough to understand the most realistic condition. Many countries have no data published in this regard and even some large countries like Pakistan and Australia have had published only less than three studies per year about pharmaceuticals in environment.

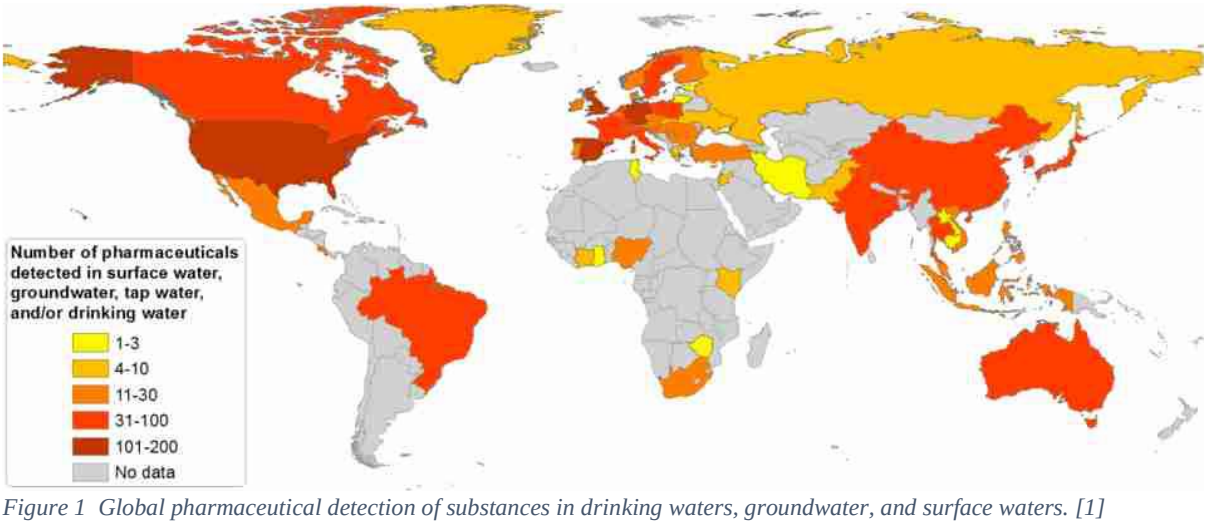

Figure 1 Global pharmaceutical detection of substances in drinking waters, groundwater, and surface waters. [1]

Since antibiotics is the one class that has been the most found in environment, according to data, consumption of antibiotics only in 2015 surpassed 34.8 billion prescribed daily doses (which is on average the required maintenance doses/day for one drug or DDD, used in adults. This is a huge increase of roughly 65% from year 2000 where defined daily doses were 21.1 billion. This accelerated consumption rate is mostly by high population countries like by China, India Brazil, and Indonesia. Currently there are more than 3000 pharmaceuticals present in the European market alone and estimated 4000 active pharmaceutical compounds in the international market leading to annual global consumption to around ~100,000 tons/year.

1.2. Effects on environment

Pharmaceuticals mostly are highly soluble and persist in the environment causing bioaccumulation and since it is little studied but possibly have carcinogenic effects of different organisms. Pharmaceutical residues in environment can be pseudo persistent and can have long term effects on microorganism and flora and fauna. The effects of these residues can modify metabolism and interfere with hormones of species in contact and furthermore not only target one or single specie but a range of other organisms too. As these pharmaceuticals consists of variable mixtures that can cause complicated behaviour so even at low threshold concentrations, they can become very dangerous for living organisms. As these pharmaceuticals actual behaviour involves binding to unique receptors in humans and animals, a great number of organisms have similar receptors. Antibiotics on prokaryotic cells act via various mechanisms that includes inhibition of protein/ DNA/RNA synthesise similarly Nontherapeutic exposure to these residues in the environment is assumed to have more adverse effects on environmental microbes as compared living organisms. According to Khan, G. A. [2] a range of effects of antibiotic in the environment have been observed, resistance of antibiotics in bacteria and other microbial communities, alteration of gene expression, growth malfunctions in rats, fish, and other aquatic life also abnormal enzyme and protein synthesise abnormal protein and enzyme activities, and growth malformations in rats, fish, and frogs have

all been observed. The effects in induvial species combinedly affect the overall web chain, for example Diclodenac, a nonsteroidal anti-inflammatory drug (NSAID) causes intense visceral gout and kidney failure that leads to death in 5-86% white-backed vulture adults, and this indirect effect has caused to decrease 95% of vulture population, as the feed on dead livestock which is often treated with this drug. There are many such example, a few have been listed in the Table 1. Pharmaceutical's concentration is mostly in ng/l range but not much have been studied about long term effects of such exposure to drinking water.in a wastewater treatment plant in Patancheru, India, very high concentration of ciprofloxacin 31 mg/L was released in the environment which is almost 44kg/day that is almost equivalent to consumption of Sweden's entire population for 5 days [3]. Such a high amount is a serious risk to both humans and local microorganisms. These bacteria enter human bodies through drinking water and other food sources such as vegetables, plants, meat and fish. As this induvial pharmaceutical might not be very harmful but when combined in a pool of different drug residues, they raise serious questions for human consumption. Another important perspective is that we know already many bacteria have become resistant to new medicine and there is always need of production of new antibacterial drugs, these antibacterial residues in the environment can increase resistance of many kinds of bacteria in the environment.

Table 1 Effects of pharmaceuticals on non-target organisms (Patel et al, 2019)

Pharmaceuticals and references	Uses	Nontarget organism	Effects	Study type
Ciprofloxacin	Human and animal antibiotic	Cyanobacteria, Green algae,	Growth inhibition	Laboratory study
	pharmaceutical	Duckweed		
Deltamethrin	Veterinary antiparasitic	Chironomids	Larvae killing in sediments	Laboratory study
Diclofenac	Human analgesic	Vultures	Population decreases	Environment effects
Diclofenac	Human analgesic	Rainbow trout	Renal lesion and alterations of gills	
Diclofenac	Human analgesic	Rainbow trout	internal organs damage	Laboratory study
Enrofloxacin	Veterinary and human	Cyanobacteria, Green algae,	Growth inhibition	Laboratory study
		Duckweed		
Ethinylestradiol	pharmaceutical hormone for humans	Carp	Changes in male to female features	Environ mental effects
Ethinylestradiol	pharmaceutical hormone for humans	Fathead minnow	Reproduction decline	Laboratory study
Ethinylestradiol	pharmaceutical hormone for humans	Fathead minnow	Population decreases	Field test
Ethinylestradiol	pharmaceutical hormone for humans	Zebrafish	Alterations in male gonads	Laboratory study
Fluoxetine	Antidepressants for human	Leopard frog	Tadpole development disorders	Laboratory study
Ivermectin	Animal antiparasitic	Benthic meiofauna	species composition shift	Mesocosm study

2. Literature review

2.1. Adsorption for removal of CIP

Adsorption is a well-established separation technique widely used in removal of organic compounds like synthetic chemicals dyes etc. It is a low investment technique that requires only absorber design, it is easily operational, and a wide range of economical adsorbents can be utilized according to the need of the process. Adsorbents can be obtained from industrial, agricultural waste to cheap and abundant natural materials. Lots of research has been going on to make use of cheaper and efficient adsorbers for various industrial applications. Many studies have been assessed to study adsorption capacity of different adsorbents for removal of pharmaceuticals from water. It has been observed that hydrophobic pharmaceutical residues have higher affinity for adsorbents whereas hydrophilic ones are not easily adsorbed. More studies need to be done in studying the mechanism for adsorption process of pharmaceutical. Various studies have been done on adsorbents like activated carbon, silica, clay etc.

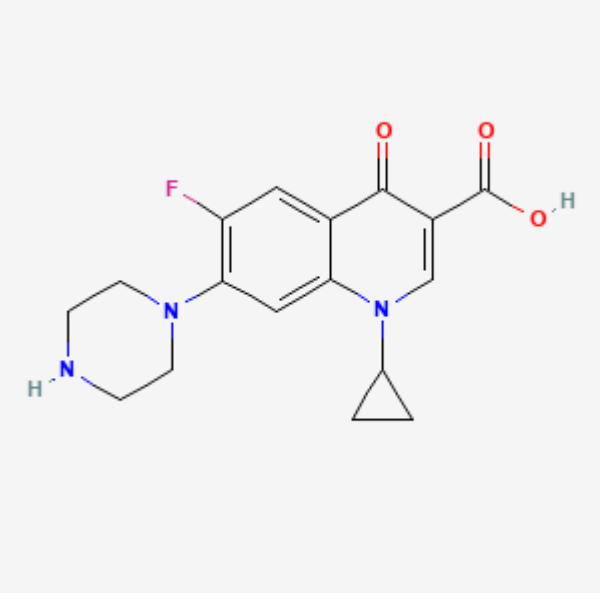

Figure 2 Structure of Ciprofloxacin [4]

The effects temperature, pharmaceutical concentration pH and ionic strength has been studied. The purpose of my thesis is specifically to study biochar as an adsorbent for adsorption of a particular CIP. Quinoles is an important group of antibiotics used in treatment of both human and veterinary diseases as it has ability to control infections both Gram (+) and Gram (−) bacteria. 70% of the Quinolone class antibiotic used is excreted out of human body unmetabolized and it has been detected frequently at sub-inhibitory concentrations in the range from ng L^{-1} to µg L^{-1}, which can then accumulate and persist in the environment increase long-term exposure. Therefore, Quinolone group can particularly change the local microbial populations in water and soil [5]. Numerous studies have been done to treat water contaminated with antibiotic Ciprofloxacin such as Ultrafiltration (UV), biological processes, radiation, sand filtration, membrane filtration and sedimentation [6]. Adsorption and biodegradation have been more popular among these techniques in last few years. Many studies have been done to analyse different materials which can be used as adsorbents for antibiotic Ciprofloxacin, most of the adsorbents are studied on a range of factors like pH dependency, multifunctionality, production and maintenance costs and regeneration. There are many types of adsorbents that have been studied for adsorption of class Quinolone antibiotic that include activated carbon (co-adsorbents like paper sludge), carbon nano-tubes, graphene oxides, clay, metal organic framework (MOF) etc. focus of my work would be biochar as adsorbent for removal of antibiotic.

2.2. Biochar as an adsorbent

Biochar is a predominantly carbon material which is achieved by thermally or hydrothermally processing biomass at heated at higher temperature with little to no oxygen supply [7]. This biochar can be further modified to improve its adsorption properties. Modified Biochar can be obtained by further activating biochar to change their surface area, pore structure and functionality. Raw or unmodified biochar's doesn't have ability to adsorb selectively high concentrations. Modified Biochar are enriched with surface functional groups that can enhance sorption capacity. Furthermore, in environmental remediation numerous methods of modification including impregnating metal oxides, surface oxidation, and functionalization have been used to enhance their performance in application of environmental remediation. Therefore, modified Biochar can be used are much effective sorbents for separation organic

and inorganic contaminants in water [8]. Modified biochar could have a limited surface sorption capacity so a long term a contact with the sorbate molecules consequently results in thermodynamic equilibrium between sorbates and sorbents hence regeneration of sorbents for the purpose of reuse or disposal is necessary. There's always a need for economical and effective regeneration method which can reduce the cost significantly and increase reusability of biochar adsorbents, it can be done by using HNO_3, KNO_3 or $NANO_3$ at varied concentrations. Such reusability makes biochar adsorbent much more economical.

Some studies have been done on removing ciprofloxacin by biochar (BC). The application of biochar in removal of ciprofloxacin has been challenging because of its environmental speciation. For most of the adsorbents been used for antibiotic ciprofloxacin, adsorption affinity is only favourable in a small pH range, or the adsorption is decreased with the increasing in the negative surfaces of the adsorbents with pH increase. Solution to these short comings is multi-functionality sorbent, biochar [9]. A thermally modified reed straw biochar composite consisting of pyrite and hematite removed ciprofloxacin with a high capacity of 345 mg g^{-1}, which is 2-times higher than that of the simple BC, meaning multi-layered adsorptive removal was done with a good Freundlich model. same pH effects were observed for biochar produced from camphor leaves with maximum adsorption at pH 5.5–6.

Many types of biochar adsorbents have been used for ciprofloxacin treatment and their sources range from reed saw, rice straw, sugarcane bagasse, potato leaves, camphor leaves, pomelo grapefruit, municipal solid waste, used tea leaves, cassava, cattail, vinasse. Most of these Biochar applications have been on different antibiotics of class Quinolones. For example, rice straw has been used on ciprofloxacin, and optimal pH for high chemo-adsorption has been between 6-8, with maximum adsorption per gram of adsorbent been 52.75. [10]. BCs have with diverse oxygen containing functional groups such as the hydroxyl (-OH), carboxyl (-COOH) and benzene-rings, which are important for Quinolone's antibiotics uptake [11]. As biochar is produced from pyrolysis at high temperatures up to 500◦C, aromatic groups increase and there is loss carboxyl and hydroxyl groups. This enables the electron donors and acceptor presence on the adsorbent surface, which further increases interaction between with the like part of the class Quinolones.

Table 2: Conventional treatment processes for pharmaceuticals (Patel et al, 2019)

Treatment processes	Advantages	Disadvantages
WWTPs (Activated sludge treatment)	• High sorption coefficients pharmaceuticals are removable with sludge • Less costs for operations and maintenance	• Low efficiencies for removal of pharmaceuticals • Production of large quantities of sludge
Constructed wetland	• High removal performance of different contaminants including a large range of pharmaceuticals • Low costs in energy consumption and operations and maintenance	• Needs large area of lands and long retention time • Inefficient removal of a large range of pharmaceuticals
Chlorination	• Only removal of compounds containing highly reactive (hydroxy-substituted aromatic structures) with more than 90% efficiency	• Low efficiency of removal of most pharmaceuticals • Generation of chlorinated byproducts for the environment
Membrane bioreactors	• Effective in calcitrant compounds removal that include high efficiencies pharmaceuticals	• High costs of energy and maintenance of membranes, aeration etc • Not efficient with the removal of a large number of pharmaceuticals
Microfiltration/ Ultrafiltration	• Effective removal for some pharmaceuticals • Good removal of pathogens and some metals	• Low removal of pharmaceuticals • Not entirely effective with removal of some pharmaceuticals depending on pore size which varies from 100 to 1000 times and is greater than micropollutants
Nanofiltration	• Efficiently removes organic pollutants like pharmaceuticals	• High operation cost in term of membrane fouling, energy consumption and water disposal • Only limited removal of pharmaceuticals
Reverse Osmosis	• Reduces volume of wastewater and 90% of large EDCs are removed	• High energy consumption costs and membrane fouling

3. Problem statement of the thesis:

Antibiotics accumulation in the environment is no more a problem of future, pseudo accumulation has a negative impact on the environment and eventually to human beings. It also adds up to the challenge of antibiotic resistance the world is already struggling with. A report [12] shows that Oslo's two main hospitals, have a high discharge of pharmaceuticals into wastewater especially Paracetamol and Ciprofloxacin. Two main hospitals waste is connected to a large wastewater treatment plant, Vestfjorden Avløpsselskap (VEAS) which has recorded borderline alarming concentration of Ciprofloxacin in its sludge. The problem arises as this sludge is used as a fertiliser, the possibility of such drugs travelling back in food chain can be very dangerous. The target is capturing the problem at its source and treatment of drugs at hospital waste rather than upgrading existing WWTP is more beneficial. Biochar from wood and sludge is already a waste and utilising it as an adsorbent plays important part in circular economy. Biochar is cheap, easily available and has the required characteristics for a good adsorbent and initial literature review shows it as a great protentional to contribute to solving the problem of pharmaceuticals pollutants in wastewater. Main objective of this thesis is to characterise different properties of biochar and perform batch adsorption with Ciprofloxacin. Analyse results and find out ideal conditions and pyrolysis temperature that give the optimum performance further.

2 Materials and methods

2.1 Materials

In this thesis 9 samples of biochar were used, four from wood and 5 from sludge pyrolyzed at different temperatures. (Table 3). All biochar material was supplied by Scanship As.

The wood samples come from pellets of softwood, 60/40 by volume of Norway spruce (Picea abies) and Scots pine (Pinus sylvestris). These pellets were made from whole tree trunks including bark, inner bark, cambium, sapwood, and heartwood. The samples were produced by batch scale Biogreen pyrolysis unit containing an electrically heated screw (Biogreen, 2021). The samples were heated at different temperatures between 500°C and 800°C.

For sludge Lindum/Vesar wastewater treatment plant was collected and sent to bio-sludge treatment system to reduce material volume through first dewatering and then drying. After the moisture content in source sludge is reduced to acceptable percentage which is about 15% or lower. The dried sludge is heated in the full or partial absence of air under variable.

Table 3 Samples of biochar adsorbent obtained from wood and sludge at different pyrolysis temperature

Wood	Sludge
WPB- 550°C	BRLB-500°C
WPB- 600°C	BRLB-600°C
WPB- 700°C	BRLB-700°C
WPB- 750°C	BRLB-800°C
	BRLB-15% Moisture(un-pyrolyzed)

Methods

2.1.1 Characterization Techniques

The different samples of biochar adsorbent as shown in Table 3 obtained from wood were analysed by using various analytical methods for the identification of soil content, crystalline structure, functional groups, thermal stability, surface area and pore volume.

The following are the characterisation approaches utilized in this research:

- Attenuated total reflectance-Fourier transform infrared (ATR-FTIR) spectroscopy
- Powder Xray Diffraction (PXRD)
- Thermogravimetric analysis (TGA)
- Brunauer-Emmett-Teller (BET)
- Ultraviolet visible (UV) spectroscopy

2.2 XRD

XRD is a strong non-destructive technique for analysing crystalline samples. The atoms in the crystalline substance repeat in a regular and distinct pattern. An amorphous (non-crystalline) substance will not refract, whereas a substance with any crystallinity, even if blended with amorphous substance, will diffract [13]. Structure, texture, phases, and other structural data like crystallite size, crystallinity, stress, and crystal defects are measured by XRD. The constructive interference of a monochromatic beam of X-rays dispersed at certain angles from each pair of lattice planes in a sample produces XRD peaks. The arrangement of atoms inside the lattice determines the peak intensities. As a result, the fingerprints of periodic atomic configurations in a specific material are the X-ray diffraction patterns.

Procedure

X-Ray diffraction system contains a catalyst holder, an X-ray generating source, and X-Ray detector that can spin at an angle θ. The sample held in a sample holder may be exposed to X-rays from the X-Ray source. The sample absorbs a portion of the X-ray beam, which is subsequently propagated and diffracted. The sample absorbs a portion of the X-ray beam, which is subsequently propagated and diffracted. The diffracted beams are detected by the XRD detector, which sends electrical impulses to the computer and generates the XRD spectra according to the signals received. When X-rays contact the surface of a crystalline material, they are partly dispersed by atoms. The non-scattered part of the X-ray travels to the next layer of atoms, where half of the X-ray is dispersed and half travels to the next layer. Similarly, to how a grating diffracts a light beam, this results in a substantial diffraction pattern. The specimen should be crystalline as well as the distance among atom layers must be closer to the radiation wavelength for an X-ray to refract [14]. When beams refracted by two separate layers are in phase, constructive interference occurs and a peak appears in the diffraction peaks; conversely, if they're still in phase, destructive interference happens, and no peak appears. Diffraction peaks appear only when Bragg's Law is fulfilled:

$$2d\ sin\theta = n\lambda \qquad (1)$$

Where,

d= distance between planes of atoms

θ= Angle between X-ray beam Crystal plane

n= X-Ray diffraction integer

λ= Wavelength of X-Ray used

PXRD testing was conducted via Bruker D8 Advance with a Cu-Kα source of radiation (λ= 0.154 nm). The materials were finely crushed using a pestle and mortar before being placed on a specimen holder (sample specimen Ø 25 mm and PMMA=8.4 mm height). During sample preparation, samples was properly crushed to make fine particle, it was further compressed using a thin glass plate and a razor. The X-ray tube was activated with a power of 25 mA and a voltage of 40 kV. One of the most essential analytical methods for confirming the presence of crystalline chemicals in Biochar is PXRD. All of the synthesized samples were evaluated for 2Θ = 2° to 70° using a 0.0103° step size and a scan speed of 5.85°/min. The information was saved as XY-files and plotted in QTI plot. Figure 3 depicts representation of X-ray diffraction from crystalline phase.

Figure 3Schematic diagram of XRD from crystal planes

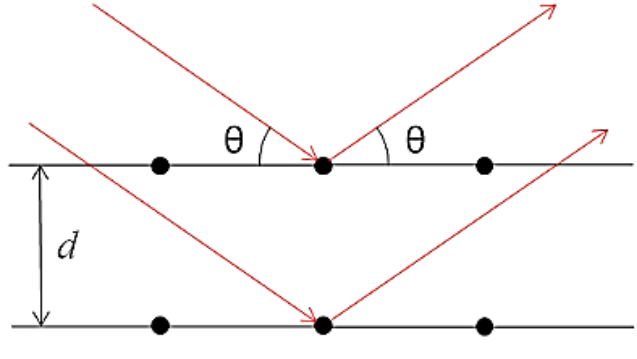

2.3 ATR-FTIR

ATR-FTIR is a sampling technique used in conjunction with conventional IR spectroscopy that allows specimens to be viewed immediately in either liquid or solid condition. FT-IR is a method for obtaining an infrared spectrum of a solid, liquid or gas sample's emissions or absorbance. The presence or disappearance of various functional groups, and the chemical nature and structure of a of compound can be determined using FTIR–ATR. An IR spectrum gathers high-resolution spectral data concurrently over a wide range. This is preferable to the typical dispersive spectroscopy, which only detects spectral intensities over a much narrower wavelength ranges at any given time. The term 'FTIR spectroscopy' refers to the process of converting raw data into spectrum using the Fourier transform. FTIR analysis was employed to examine and define vibrational present on the surface using IR radiation on the sample material Since IR-radiation is employed, black substances such as carbon, charcoal and biochar can absorb light completely, yielding in less usable spectroscopic results[13, 15].

Procedure

An ATR accessory works by detecting changes in an internally reflective IR beam when it gets into touch with a material. At a specific angle, an infrared beam is transmitted onto an optical dense crystal with a higher index of refraction. This internal reflection generates an acoustic wave that spreads beyond the crystal's surfaces into the material in touch with it. The evanescent waves will be dampened in parts of the Infrared spectra where the specimen absorbs the energy. The attenuated beam travels to the crystal, then leaves the opposite end of the crystal and is guided to the IR spectrometer's detector (Figure 4). For biochar characterization, Agilent Cary 630 Spectroscopy was used to obtain IR spectra. Before each experiment, an empty background spectrum was acquired. Very little part of the powder samples was crushed and deposited on base of the diamond. The base of the crystal was cleaned with soft and dry paper between measurements.

The ATR-IR spectrum were obtained between 400–4000 cm^{-1} at room temperature with 32 scans per spectrum. The data was saved as XY files and plotted using QTI plot.

Figure 4 Schematic representation of FT-IR

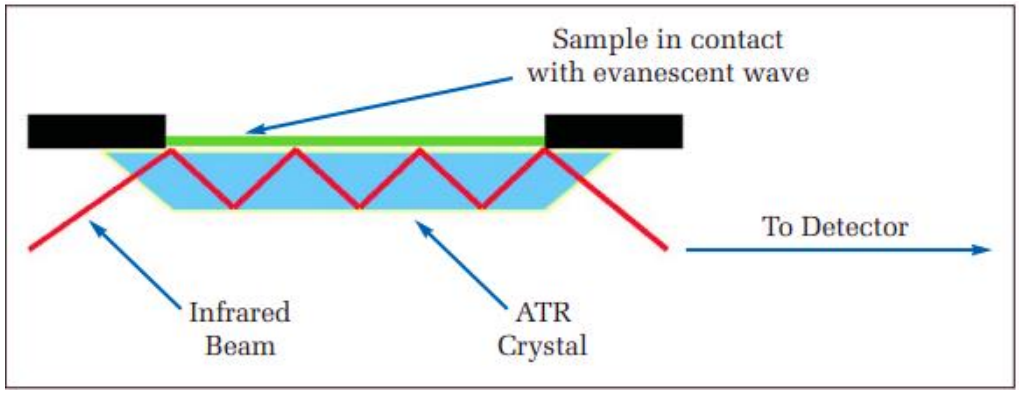

2.4 TGA

Thermal analysis (TA) is one of the characterisation techniques use to observe and measure changes in test material physical and chemical properties like mass, volume, structural changes etc with change in temperature under controlled condition [16]. The conditions can vary along with temperature, it could be vacuum, inert, oxidising/reducing conditions. Thermogravimetric analysis (TGA) is specifically used to study changes in mass with change in temperature. A small amount of mass using very sensitive six-digit balance, the samples is placed in a furnace with a pre-set program. The furnace provides a space around the samples which can be changed according to the requirement of program, inert N_2, Ar, He, or synthetic air can be added [17].
This technique can be used to study thermal stability of a sample, activation temperature, important fuel properties like volatile matter, carbon, and ash content. For example, for biochar it could be found out at what temperature does moisture and its solvent content disappears from the sample, which is generally the first plateau on mass loss vs temperature graph. Similarly, thermal stability can be determined when there begins to be change in mass of a sample.

Procedure

To perform TGA analysis, Mettler Toledo TGA apparatus was used. All nine samples were measured and added into an aluminium oxide crucible in the apparatus. The mass was measured around 4.50mg of each. The samples were heated from 25°C to 900 °C under 25 mL/min of N_2 and in second part 900°C of 25mL/min of synthetic air flow. The heating grate was fixed at 10°C/minute. Under isotherm condition of 900°C the procedure was performed until the mass became constant. The data was

exported as an XY file for each sample and two graphs of weight-loss% vs temperature (25°C to 900 °C) for first part and weight loss% vs time (for 900°C) for second part were plotted on QTI plot.

2.5 BET

BET theory seeks to explain the physisorption of gas molecules on a solid substrate and form the basis for an essential analytical method for identifying the surface area of porous or solid materials. BET theory is used to determine the specific surface area in the multi-layered sorption process, and it typically uses penetrating gases i.e., nitrogen (N_2) or argon (Ar) at 77 k which do not react chemically with material surfaces as adsorbates. N_2 gas (adsorbate) is applied in regulated quantities to the sample material (adsorbent). After each dose of N_2 gas, the relative pressure (P/P_0) is allowed to settle before determining the monolayer capacity n_m of adsorbed nitrogen. The BET equation precisely defines a linear plot of $1/((P_0/P)-1)$ vs. P/P_0, which is constrained to a limited area of the isotherm models for most solids employing nitrogen as the adsorbate, typically in the P/P_0 range of 0.051-0.34. The following BET Equation 4.1 is used to compute the n_m from the sorption isotherm model [18, 19]:

$$\frac{1}{n\left(\frac{P_o}{P}-1\right)} = \frac{1}{n_m C} + \frac{C-1}{W_m C}\left(\frac{P}{P_O}\right) \qquad (4.1)$$

Where,

n= adsorbed amount

C= constant that indicates the amplitude of the favourable adsorbent/adsorbate interaction

P_0/P= relative pressure

n_m= monolayer capacity

The Equation 4.2 can be used to compute the sample's total Surface area.

$$S_t = \frac{n_m N_A}{V} \qquad (4.2)$$

Where,

S_t= sample’s total surface area

n_m= monolayer capacity

N_A= Avogadro's constant

V= molar volume of adsorbed gas

The amount of gas adsorbed by a porous material at a constant temperature as a function of pressure is represented numerically by an isotherm model. Porous materials are most commonly described in terms of pore sizes determined from gas sorption data, and IUPAC conventions for categorizing pore sizes and gas adsorption isotherm that represent the link between permeability and sorption have been developed. Figure 5 depicts the IUPAC classifications of adsorption isotherm models. Type I isotherms are employed to characterize sorption on microporous adsorbents because they 'reach a limiting value' [4]. Adsorption on macro-porous adsorbents with weak and strong adsorbate/adsorbent interactions is described by Types II and III, correspondingly. Types IV and V represent monolayer and multilayer adsorption as well as capillary condensation. Type VI, which was excluded from the Brunauer classification, demonstrates that adsorption isotherms can have one or more stages [20].

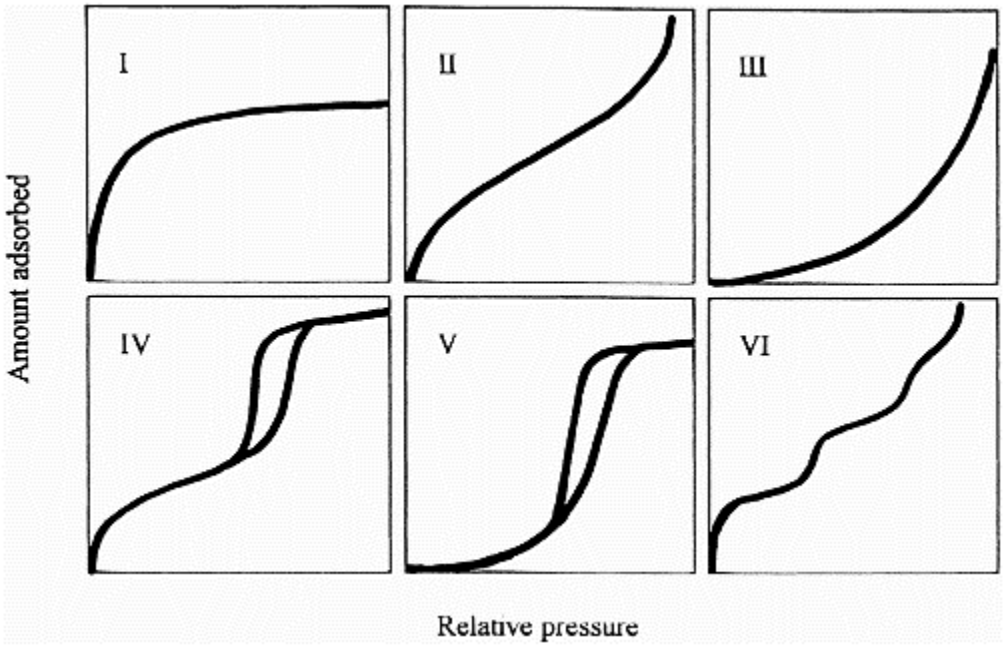

Figure 5 . The IUPAC Classifications of Gas-Solid Equilibria Adsorption Isotherm models

2.6 Nitrogen Sorption

Micromeritics® TriStar II Plus was used to conduct nitrogen adsorption. The mass of the individual tube and the rubber cap was calculated and recorded. For each adsorbent, approximately 0.12 - 0.14 g were weighed and placed within the cell. The samples tubes were heated for 250°C for 3 hours under vacuum, through which moisture was removed. After activation tubes masses were remeasured and difference was recorded which was later used for calculations. These tubes were then put in BET equipment to begin the process. The nitrogen sorption experiment was carried out at 77 K. The data were generated as an XY file and used to plot in QTI plot.

2.7 Carbon dioxide sorption

The BET method frequently relies on the adsorption isotherms of N_2 and Ar at their corresponding boiling points. However, because particles cannot exceed the activation energy for moving through the pores at extremely low temperatures, it is difficult to quantify nitrogen and argon isotherms at 77 K and 87 K if some materials contain "tiny" ultra-micropores near the kinetic diameters of N_2 and Ar. In those cases, the CO_2 adsorption-desorption isotherm models have been explored for ultra-micropores where N_2 and Ar cannot be accessible at cryogenic temperatures. Although the surface area estimated via CO_2 adsorption-desorption isotherms is not considerable due to strong CO_2-CO_2 interaction, it is an alternate method for determining surface area by applying BET theory. Because CO_2 has a relatively high vapor pressure (3.5 MPa) at 25^0C, the pressures necessary for micropore size investigation are in the medium range (0.1–100) kPa. Diffusion is substantially faster at these relatively elevated temperatures and pressures, and pores < 0.4 nm can be reached. However, because the easily quantifiable highest relative pressure for CO_2 at 25^0C is $P/P_0 \sim 3 \times 10^{-2}$ (equivalent to ambient pressure), only pores <1 nm can be investigated. CO_2 adsorption at 273 K has become a widely used approach for researching carbon-based materials with very small micropores. However, CO_2 is not suggested for pore size measurement of micro-porous solids with polar surfactant molecules (e.g., oxides MOFs, and zeolites,) because CO_2 has a greater quadrupole moment than N_2, making it difficult to link the CO_2 pore filling pressures with pore size. The method described in the literature [21] is to study the use of BET analysis for determining the surface area of samples using CO_2 isotherm.

Procedure

The procedure for carbon dioxide sorption is similar to nitrogen sorption. The measurement of mass is done in the similar way and carbon dioxide is used instead of nitrogen gas. Since carbon dioxide sorption is done at zero degrees Celsius, dewar is filled with slurry of dry ice and water in ratio of 2:1. the slurry should not be filled with excess water it may not maintain the temperature and adding too much dry ice could hinder the entrance of tubes and can even break in case, so that needs to be taken care of.

2.8 Ultraviolet-visible (UV) spectroscopy

Ultraviolet-visible (UV) spectroscopy is a profound tool in analytical chemistry. It has wide application in clinical and chemical laboratories. It is basically used for identification of chemicals and their qualitative analysis, but its major application lies in for determination of quantities of different inorganic and organic compounds present in a solution.

Spectroscopy is performed on the basics of interaction between light and matter. When matter absorbs light, it results in an increased energy level of the atoms/molecules, this absorption of ultraviolet or visible light by any chemical compound produces a unique spectrum. When UV radiations are absorbed by a solution, it causes the excitation of the electrons from the ground to an energy state. According to the theory of this concept the energy absorbed from the ultraviolet radiation equals to the difference of energy in the higher and ground state energy [22].

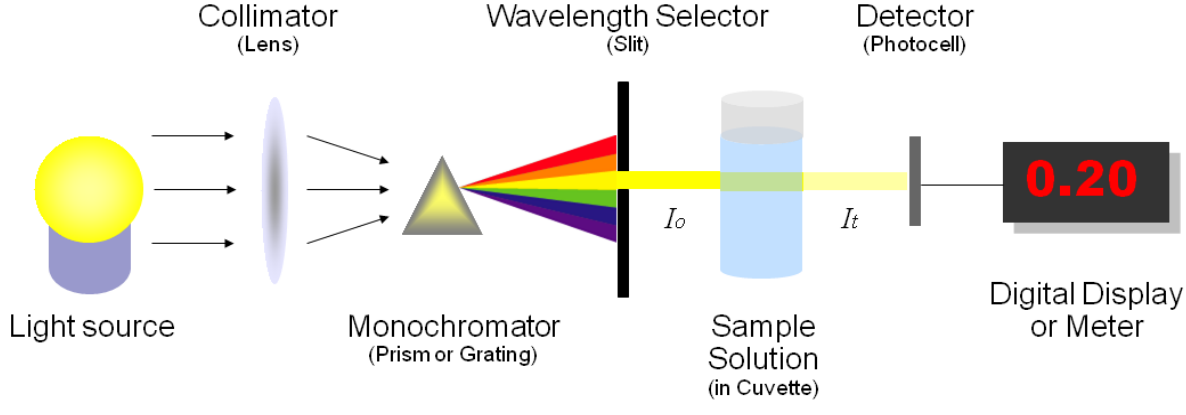

Figure 6 . Schematic representation of UV spectroscopy

Principle of Ultraviolet-visible Spectroscopy

Ultraviolet-visible spectrophotometer follows Beer-Lambert Law. The law says that when a beam of monochromatic light beam is passes via a solution having an absorbing substance, the rate of radiation

decrease alongside the thickness of absorbing substance in the solution is proportional to incident radiation and the concentration of the solution.

The law equation:

$$A = \log\left(\frac{I_O}{I}\right) = ECL \qquad (4)$$

Where,

A= absorbance

I_0= intensity of light on the sample cell

I= intensity of light leaving the sample cell

C= concentration of the solute

L= length of the sample cell

E= molar absorptivity

From the Beer-Lambert law, it has been derived that more the number of the light absorbing molecules are light at a certain wavelength, more will be the absorption of light.

Procedure

A previously made ciprofloxacin solution of 20 mg/l was used to make six solutions of different concentrations. This solution was initially made by adding 20 mg of ciprofloxacin in 1000 ml volumetric flask, the flask was filled with distilled water still the mark. This solution was named as stock solution and would be refereed as such in the following document. This stock solution was further used to make six solutions of different concentrations. To make 6 diluted solutions, 25ml volumetric flasks were used to add a certain amount of solution from the stock solution and filled up to the mark with distilled water. To make 1mg/l solution, 1.25ml of stock solution was measured by a pipette, 25 ml volumetric flask and rest filled with distilled water. Further, these six solutions were measured for UV-spectra using UV-1600PC Spectrophotometer for wavelength of 190 nm-800nm.step 1nm, absorbance and wavelength of the spectra was noted down and a calibration curve was drawn. Secondly, the lowest and the highest concentration solutions 1mg/l and 6mg/l spectra were measured three times each and standard deviation and error were measured based on the results (Figure 7).

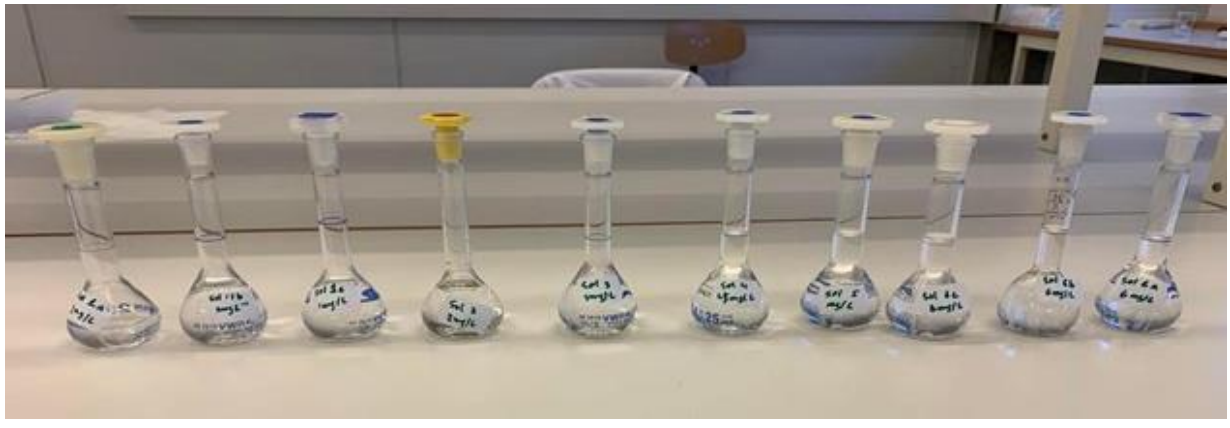

Figure 7. Laboratory picture CIP solution

Next, two more samples of the lowest and the highest dilution samples were made and measured for spectra and had done standard deviation and error calculations.

The calibration curve gives a linear relation between absorbance and concentration. Later equilibrium concentration is calculated using the Eq.4:

$$Ce = \frac{absorbance - b}{a} \qquad (4)$$

Where,

Ce= equilibrium concentration of aqueous phase

b= interception of the calibration curve

a= slope of calibration curve

2.9 Batch adsorption

For drug uptake, mass of empty glass vial with the lid was measured and approximately 0.05g of biochar sample was added in to 6 vials for one type of biochar, as there are 9 samples hence 54 glass vials were prepared. For activation, the glass vials without the lid were kept in a muffle furnace at 250°C for 3 hours. After 3 hours, the glass vials were removed from furnace and lid immediately put back on to avoid moisture getting in the sample. Mass after activation was measure and the difference between

empty glass vial was used as mass of the sample. As 6 solutions of concentration of 1mg/l to 6mg/l were prepared earlier, 20ml of each solution was added into each glass.

The vials were carefully shaken using with IKA Ms 3 basics of around 30 seconds for each glass vial and small magnetic stirrer were added in to before placing it in a water bath for 24 hours. After 24 hours, 10ml from each vial was added into centrifuge tube and placed in centrifuge machine (Eppendorf Centrifuge 5804R for) for 5 minutes under 4000 rpm. Top liquid from each tube was collected and using a syringe filter of 0.2 µm filter added to a quartz cuvette to perform UV analysis. Blank distilled water sample was run before testing for UV and quartz was washed and dried between testing each sample. All measurements were done from lowest to highest concentrations and UV peak for wavelength of 274.5 was observed and all UV data was exported to Ms excel to plot Isotherms.

Figure 8 a) IKA Ms 3 basics. B) Batch sorption setup

To plot isotherms, equilibrium concentration is calculated using Eq.5 from calibration curve.

$$Ce = \frac{Absorbance + 0.0097}{0.0955} \qquad (5)$$

Where, absorbance is at 274.5 nm.

Then, absorbance capacity is calculated using mass balance equation (Luo & Deng, 2019, p. 89):

$$q_e = \frac{(C_0 - C_e)V}{M} \qquad (6)$$

where,

q_e is the adsorption capacity (mg/g)

C_0 is the initial concentration of adsorbate in the aqueous phase (mg/L)

C_e is the equilibrium concentration of adsorbate in the aqueous phase (mg/L)

V is the volume of aqueous phase (L)

M is the mass of activated adsorbent (g)

2.10 Sorption isotherm analysis:

In order to fully understand the sorption mechanism of Ciprofloxacin onto biochar two models, Freundlich and Langmuir models will be used to fit the sorption data of all the biochar isotherm, which are related to the heterogeneous and homogenous sorbent surfaces. These parameters are calculated using the following equations:

Freundlich model:

$$\lg q_e = \lg k_F + \left(\frac{1}{n}\right)\lg c_e$$

(Equation 7)

Where,

Ce ($mg \cdot L^{-1}$) is the equilibrium concentrations of CIP,

kF [$(mg \cdot kg^{-1})/(mg \cdot L^{-1})n$] is the Freundlich coefficient related to sorption capacity,

and n is Freundlich depicting the sorption intensity

$$\frac{1}{q_e} = \frac{1}{q_{max}} + \left(\frac{1}{K_L q_{max}}\right)\left(\frac{1}{c_e}\right)$$

(Equation 8)

Where,

q_e is the amount of CIP adsorbed by a mass of biochar ($mg \cdot g^{-1}$)

Ce is the equilibrium concentration in solution($mg \cdot L^{-1}$)

q_{max} is the maximum sorption capacity ($mg \cdot g^{-1}$)

K_L represents the Langmuir constant related to the bonding force of sorption ($L \cdot mg^{-1}$).

3 Results and Discussion

3.1 XRD analysis

XRD is a technique for determining a crystalline nature of a material. The spectra of biochar obtained from wood produced at 550°C, 600°C, 700°C and 750°C is shown in Figure 9. It is noticeable from the figure that two wider peaks of biochar samples at different pyrolysis temperature appeared at the 2Θ value of roughly 22.3° and 43.1° respectively. Biochar produced at 550°C has a smaller peak at 7°, as depicted in fig (a) indicating the presence of cellulose structure, but it vanishes when heated to 600°C or above, indicating a drop in crystallinity. The volatilities of the cellulose lattice were also generated by an increase in pyrolysis temperature [23, 24]. The crystallinity peaks in biochar's formed with 180 minutes of holding period were displaced to 22.3° for each sample. Due to the depletion of minerals at elevated temperature, the sharpness of these peaks reduced as the temperature rises from 550°C to 750°C. The characteristic peak of crystalline cellulose was decreased at 10° and shifted to 22.3° for WPB-550°C for biochar produced with 180 minutes of holding time and a further rise in temperature yielded in the complete vanishing of these peaks for other samples (WPB-600°C, WPB-700°C and WPB-750°C), at which cellulose framework diminished at extreme temperatures. This result suggested that the biochars were almost amorphous at extremely high temperatures and prolonged holding durations. There were no other crystalline peaks found. This is to be considered because the samples of biochar were created from wood with little mineral impurities. As a result, biochar produced between 550°C and 750°C is nearly amorphous. A wider peak was obtained at higher pyrolysis temperatures for

each sample. At elevated temperature, this suggested the establishment of atomic order in the carbonised material [25].

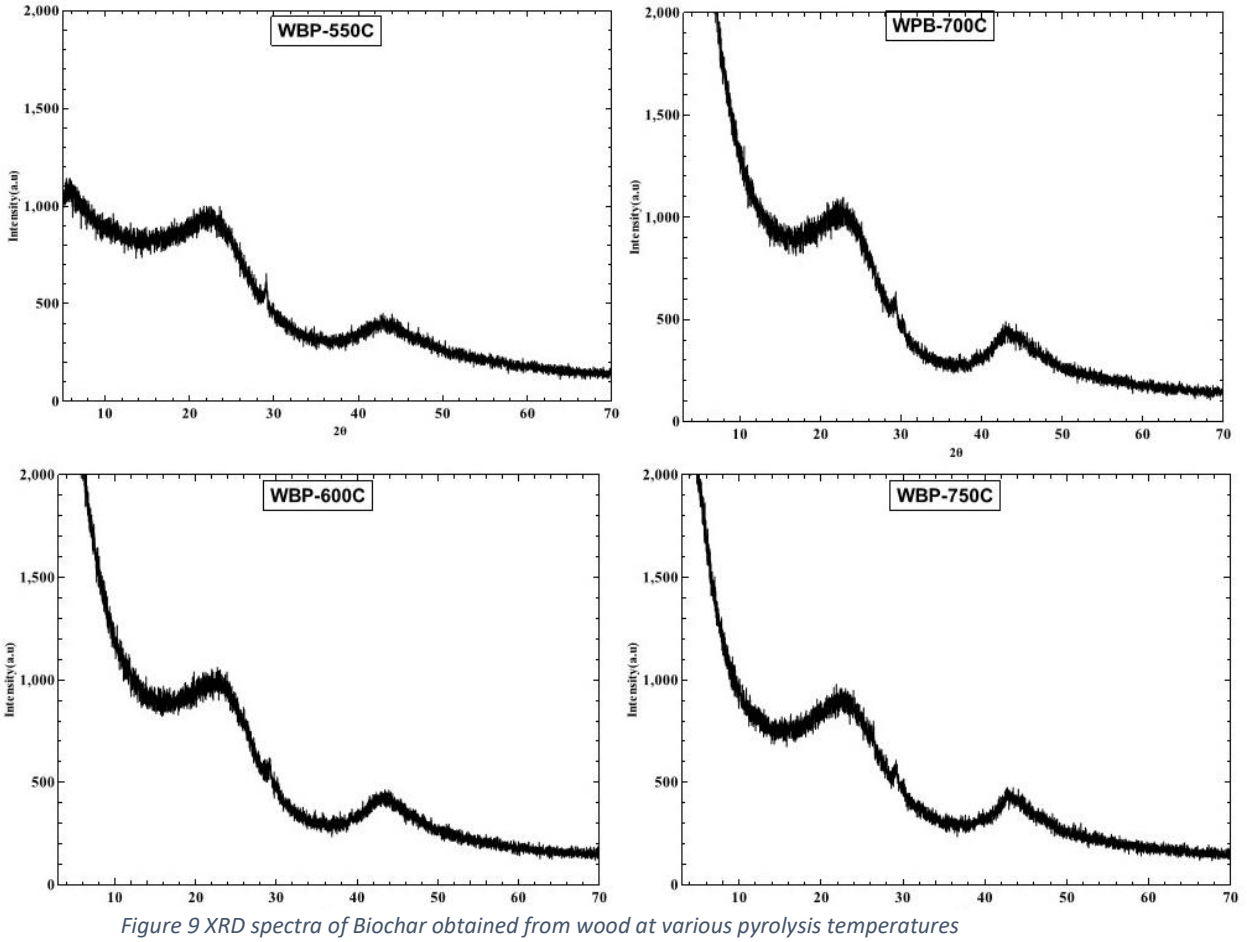

Figure 9 XRD spectra of Biochar obtained from wood at various pyrolysis temperatures

XRD patterns have been widely utilised to characterise the inorganic content of biochar and to identify the degree of pyrolysis. The generation of a broad range of crystalline and other inorganic compounds was confirmed by the XRD pattern of biochar obtained from sewage sludge generated at 500°C, 600°C, 700°C, 800°C and 15% moisture (Figure 9). In general, biochar has similar diffraction patterns at various pyrolysis temperature. Strong and sharp peak at 2Θ = 29.41° indicates the presence of inorganic compounds such as quartz, calcite, and magnetite crystals for all samples [26]. In biochar, prominent signals ascribed to minerals were found with increased inorganic content. Also, XRD examination confirmed the crystalline nature of the sample which confirmed the geometry of aromatic layers as represented by the strong peaks at the 2Θ= 25°–40°The diameters of crystal lattice perpendicular to aromatic layers are low, and this results in peak broadening [27]. For BRLB- 500°C, BRLB-600°C, BRLB-700°C, BRLB-800°C, notable sharp peaks were observed at 2Θ=34.32°, 40.91°, 42.33°, 47.36 and 51.95 were found to be maghemite (Fe_3O_4), while peaks at 2Θ=29.41° 37.62°, 39.72°and 67.56° were found to be quartz (SiO_2). For 15% moisture, sharp and strong

peak at 2Θ=29.4° showed the existence of different inorganic substances, which were linked to crystalline SiO_2, MgO and CaO forms. According to the current findings, the majority of the crystalline areas in biochar derive from cellulose crystallinity, with turbostratic crystals were extremely rare. Biochar has a heterogeneous surface, according to the Xray diffraction pattern [28, 29]. The peak intensities were reduced by increasing pyrolysis temperatures as the structure and chemical content of biochar were found to be altered by temperature [30-32]. The disintegration of minerals at high temperatures resulted in the production of new components, as shown by the fluctuation in peaks.

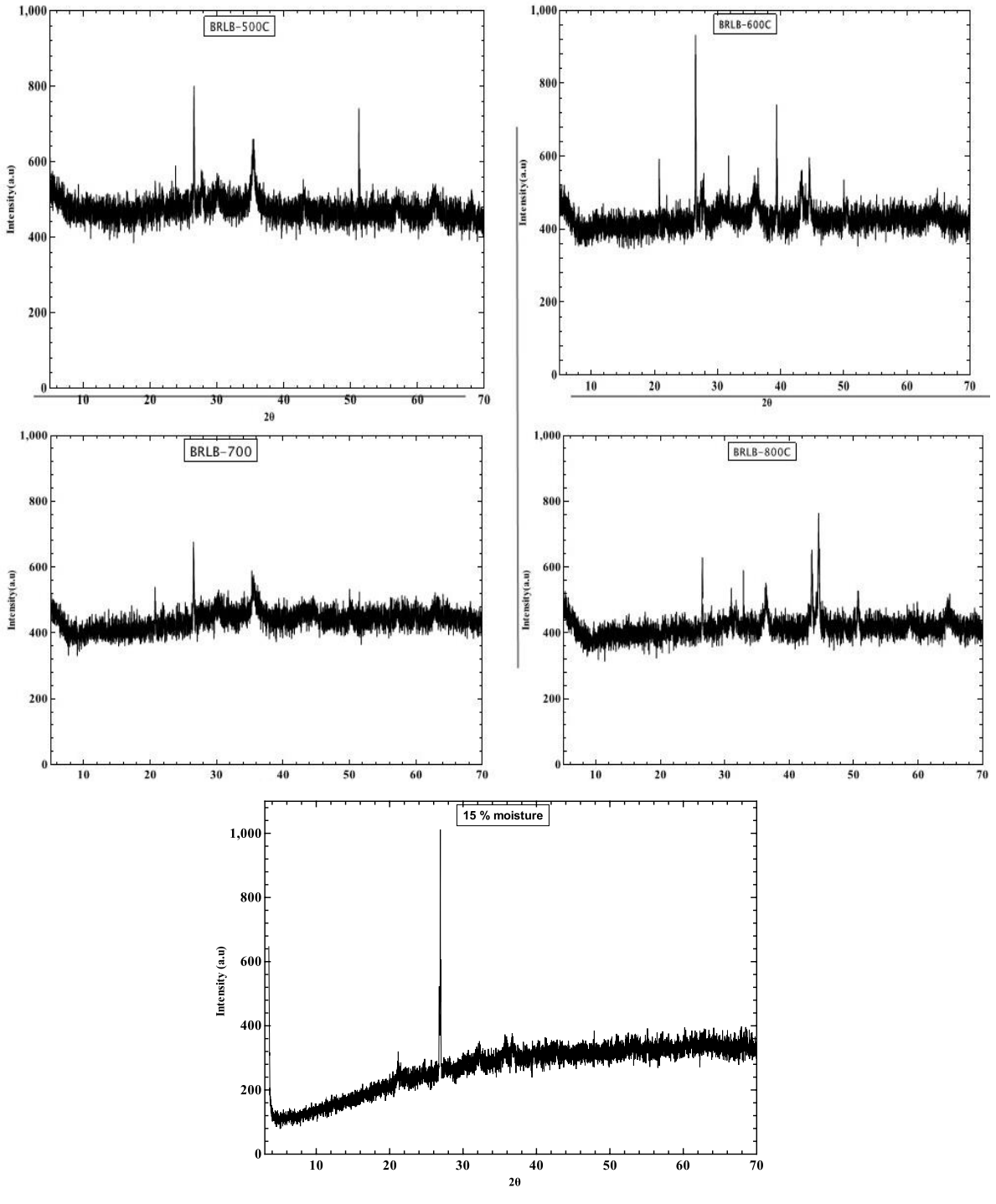

Figure 10 XRD spectrum of biochar obtained from sewage sludge at 500°C, 600°C, 700°C, 800°C and 15% moisture

3.2 FT-IR (ATR)

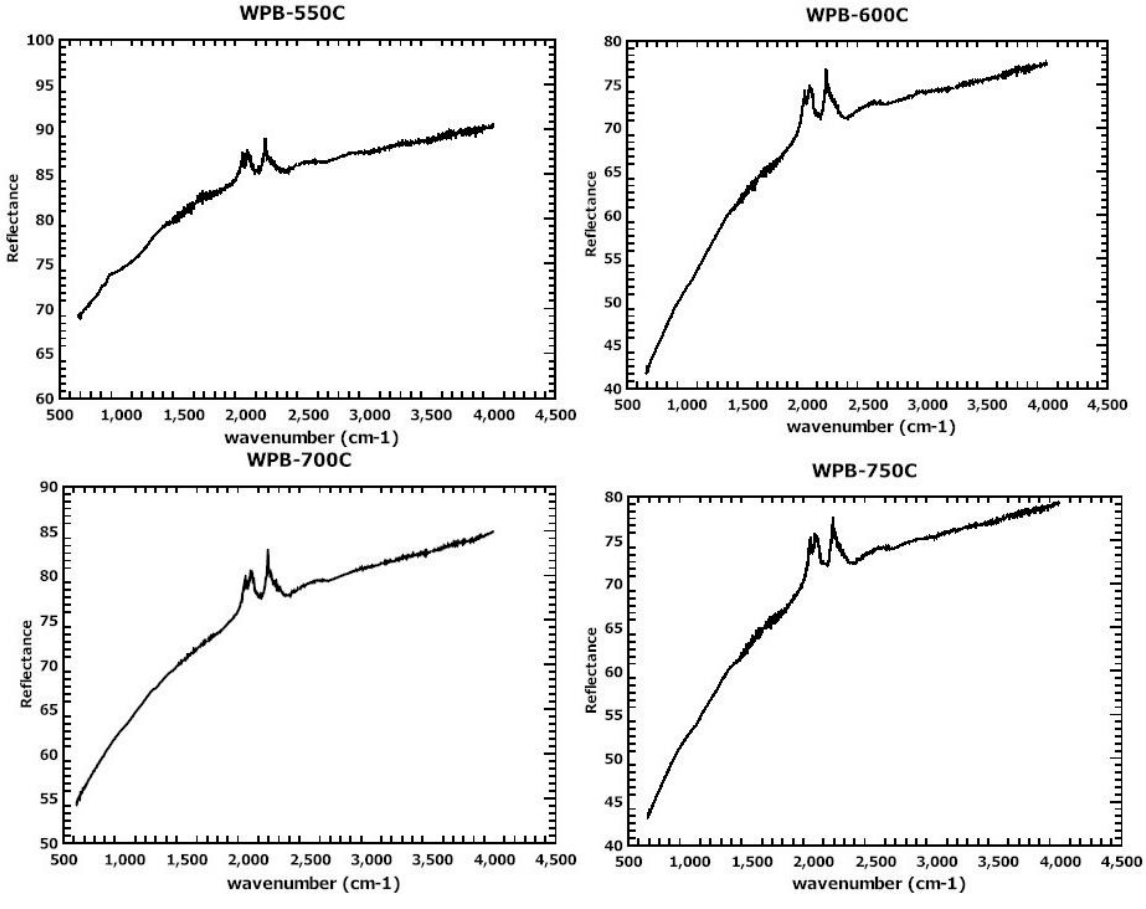

Figure 11 FTIR analysis of biochar obtained from wood at various pyrolysis temperatures

Figure 11 shows the functional groups identified by FT-IR spectra of biochar obtained from wood at different temperatures (550˚C, 600 ˚C, 750˚C). There are visible peaks at Peaks at 2261 and 2443 $cm^{-1,}$ which indicate presence of the organic residues of class C≡C for all samples. Furthermore, another prominent peaks is observed at wavelength range of 1911 to 2354 cm^{-1}, which can be associated with presence of show C=O stretching in ketene [33, 34]. In the range of 1650–1610 cm^{-1} there is no significant peak, which means absence of H-O-H bending band of water and similarly no peak in 3600–

3200 cm^{-1}, confirming ν(OH) from sorbed water and hydrogen-bonded in biochar O-H groups is absence [35]. It could be confidently concluded that wood samples have very low moisture content and this property has not been affected by pyrolysis temperature. The intensity of peaks of several biochar functional groups was reduced as the temperature was raised. The breakdown and alteration of lignin, hemicellulose and cellulose in homogenous and highly aromatic carbon materials resulted in the loss of functional groups [36].

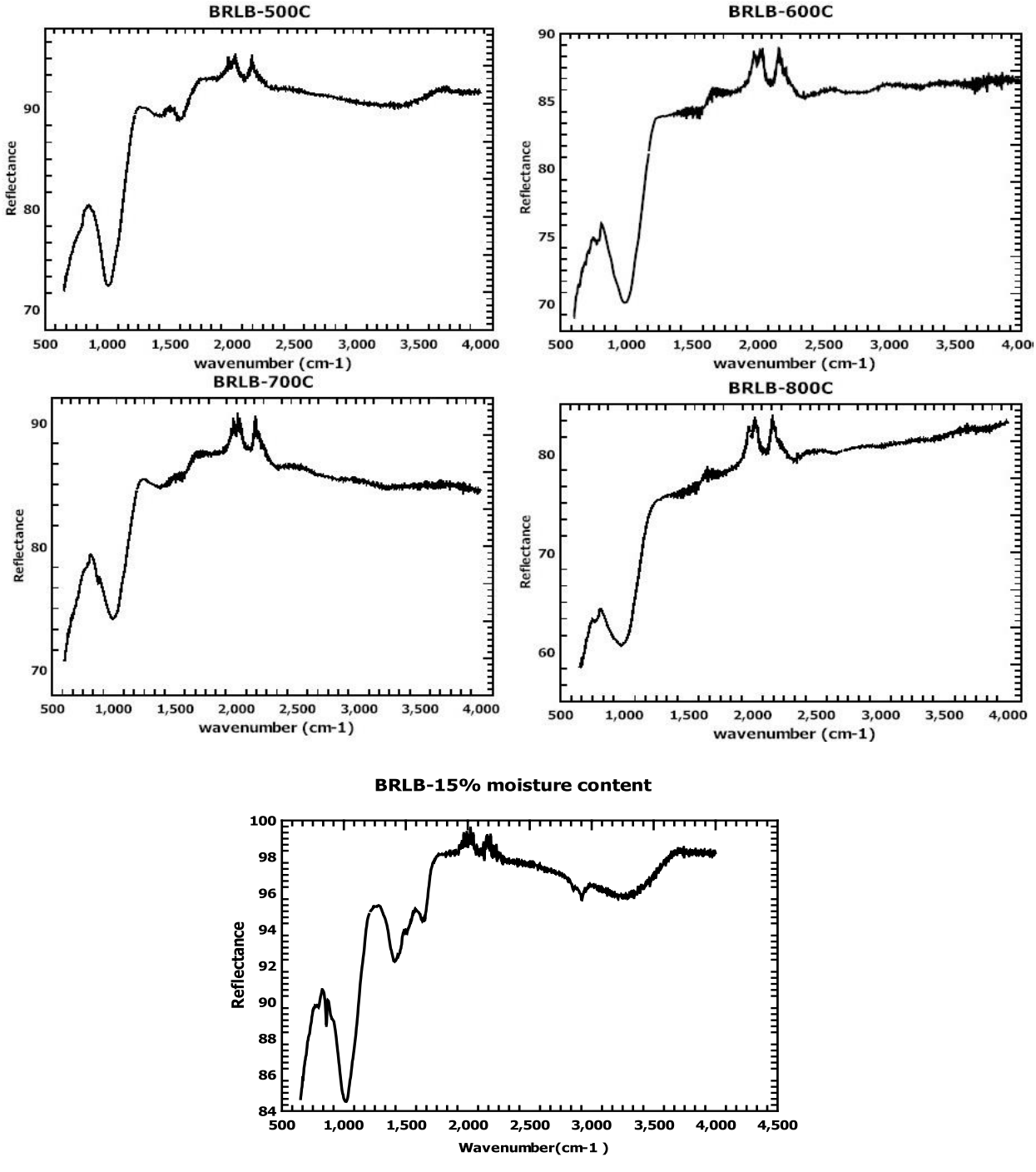

figure 12 : FT-IR spectra of biochar derived from sludge at various pyrolysis temperatures.

As displayed Figure 12, IR analysis was used to evaluate functional groups and particle surface variations in all biochar samples scanned between 500-4000 cm ^{1}. It can be seen from the spectra that biochar produced from sludge at various pyrolysis temperatures showed no significant changes. Two strong peaks at 1670 cm^{-}

^{1} and 3400 cm^{-1} exhibited -OH bending and stretching vibrations, demonstrating the moisture content at the material surface is present unlike wood samples. The bands around 1534 cm^{-1} to 1789 cm^{-1} attributed to -CH3, -CONH-, -CH_2, C=O and C=C stretching vibrations [37, 38]. Bands at 2100 cm^{-1} and 2500 cm^{-1} on the suggested symmetric and asymmetric stretching mode of methylene carbon of alkenes on surface of all four samples BRLB-500^{o}C, BRLB-600^{o}C, BRLB-700^{o}C and BRLB-800^{o}C. Peaks of aromatic carbon (C-H) at 798 cm^{-1} BRLB-800^{o}C was likewise weaker at high temperature, indicating that dehydrogenation activities were increasing.

From the current data, changes with increasing pyrolysis temperature are not as visible as in literature [39] but that could be because of variation in different types of wood, variable composition of sludge and freshness of produced biochar as well. For better understanding of this particular biochar other methods like NMR, pyrolysis GC-MS or high-resolution mass spectrometry can be applied for better understanding.

3.3 TGA

For temperature from 25°C to 900°C, changes in mass with change in temperature under inert atmosphere of N_2, where plotted in a graph off weight loss percentage versus temperature as displayed in Figure 13. The second part from 900°C, was performed under synthetic air and graph of weight loss percentage against time were plotted for all nine samples.

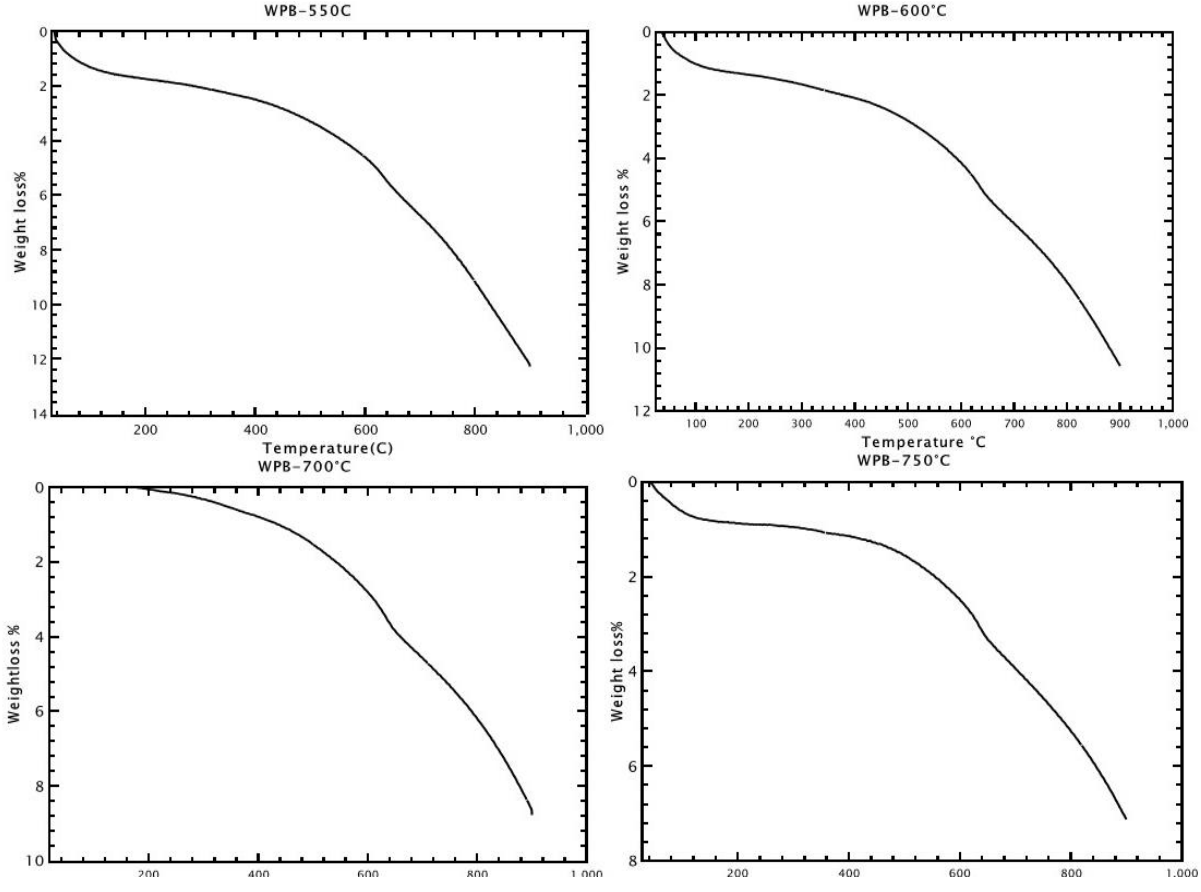

Figure 13 TGA of wood biochar samples at various temperatures under inert atmosphere with N2-flow of 25mL/min

As all the graphs depict a similar trend of increase in weight loss percentage with increase in temperature. According to [40], Loss of mass at each region can be estimated using step analysis in the following regions: loss of water from 25°C to 200°C, organic carbon loss in the 200–500°C range and the loss of carbonate in the 500–900°C range.

Table 4 Chemical composition of the wood biochar samples pyrolyzed at elevated temperatures

Biochar	Temperature (°C)	25°C-200°C Moisture (%)	200–500°C Organic Carbon (%)	500–900°C Carbonates (%)	Ash content (%)
Wood	550	1.80	1.41	10.50	3.23
Wood	600	1.38	1.40	9.05	3.48
Wood	700	0.86	0.62	7.22	3.61
Wood	750	0.85	0.61	6.55	4.32

From the Table 4, it can be seen that wood biochar samples pyrolyzed at higher temperatures have different of composition of moisture organic carbon and other carbonates. Similar to properties observed in IR spectrums wood samples have less moisture content and there is a clear trend in moisture content changing with change in pyrolysis temperature. Samples pyrolyzed at lower temperature have high moisture and it decreases with temperature increase. Wood at 550 °C have moisture content of almost 2%, and at 750°C has decreased to only 0.85%. similarly, wood at lower temperatures have high both organic carbon and carbonate content, sample one of wood has a very high almost 11% of Carbonates which fall to 6.5% at Wood 750°C.

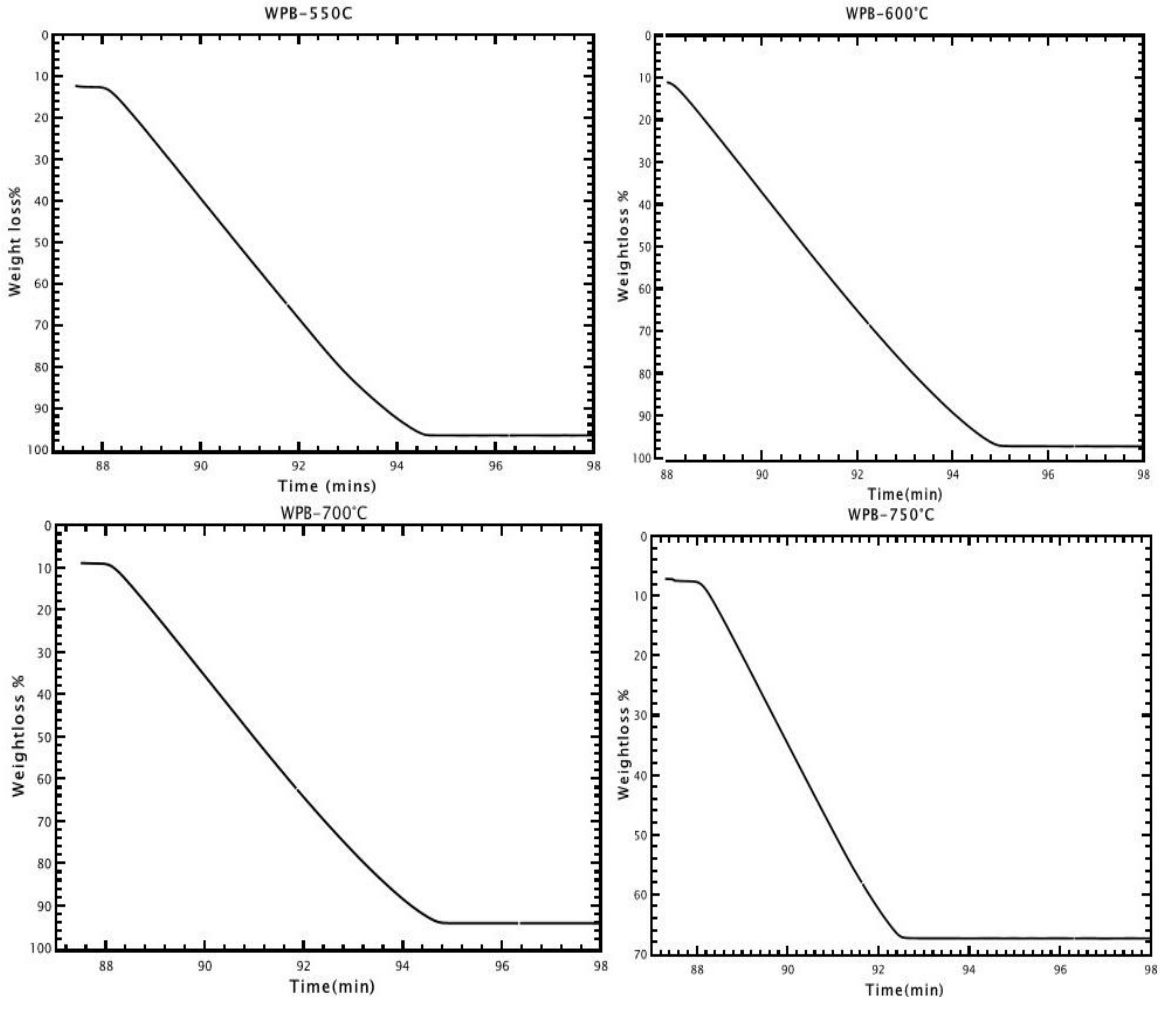

Figure 14 weight loss measurement of wood biochar samples under synthetic air flow (25 mL/min) at 900 °C

For graphs in Figure 15, the weight loss percentage was calculated as percentage of initial mass and plotted against time. There is a rapid mass loss due to combustion between wood and oxygen from air at such high temperature. The unburnt mass left is ash which requires even higher temperature to decompose completely, as ash content seems to be increasing with pyrolysis temperature, time require to reach stable weight loss% decreases.

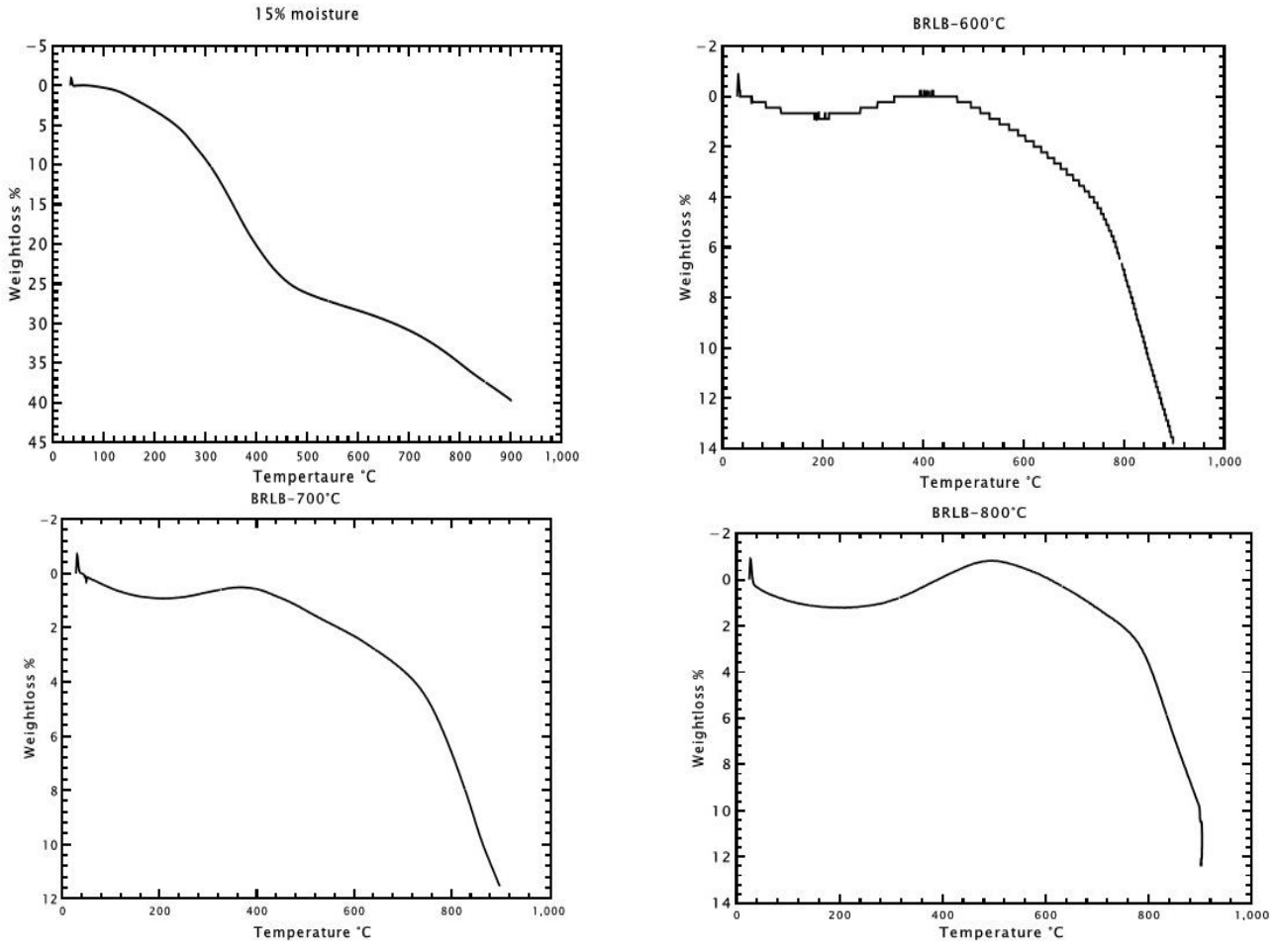

Figure 15 TGA of sludge biochar samples at various temperatures under inert atmosphere with N2-flow

For sludge samples pyrolyzed temperature 600°C, 700°C, 800°C and 15% moisture, changes in mass with change in temperature under inert atmosphere of N_2, where plotted in a graph of weight loss percentage versus temperature as displayed in Figure 15. At 900 degrees Celsius, synthetic air was introduced during and remaining biochar reacted with oxygen in the air. Figure 16 depicts the weight-loss % is plotted against time, there is rapid decrease in mass and in short time span and a mass becomes constant afterwards, as most of the matter turns into ash at this point.

Table 5 : Chemical composition of the wood biochar samples pyrolyzed at elevated temperatures

Biochar	Temperature (°C)	25°C -200°C Moisture (%)	200–500°C Organic Carbon (%)	500–900°C Carbonates (%)	Ash content (%)
Sludge	Un-processed	2.23	23.23	16.07	59.63
Sludge	600	0.89	0.52	12.99	84.9
Sludge	700	0.96	0.43	10.56	88.17
Sludge	800	1.22	0.52	11.96	88.52

In biochar samples from sludge, similar to wood samples, there is an increasing trend of moisture with increase in pyrolysis temperature. Organic and inorganics have similar weightless percentage to each other, but wood samples had a very distinct decreasing relation with temperature increase. Sludge samples have very high ash content present in all its samples and pyrolysis temperature do not have significant effect on ash content as the percentage remains almost the same for samples of different temperatures. The ash content contains inorganic oxides that require higher temperature to decompose.

The un pyrolyzed sample with 15% moisture loses most of its mass during inert gas period. As it has not been through pyrolysis before and contains high moisture, organic and carbonate content. The samples show a steep weight loss and up to nearly 50% before reaching 800°C and has less ash content as compared to others.

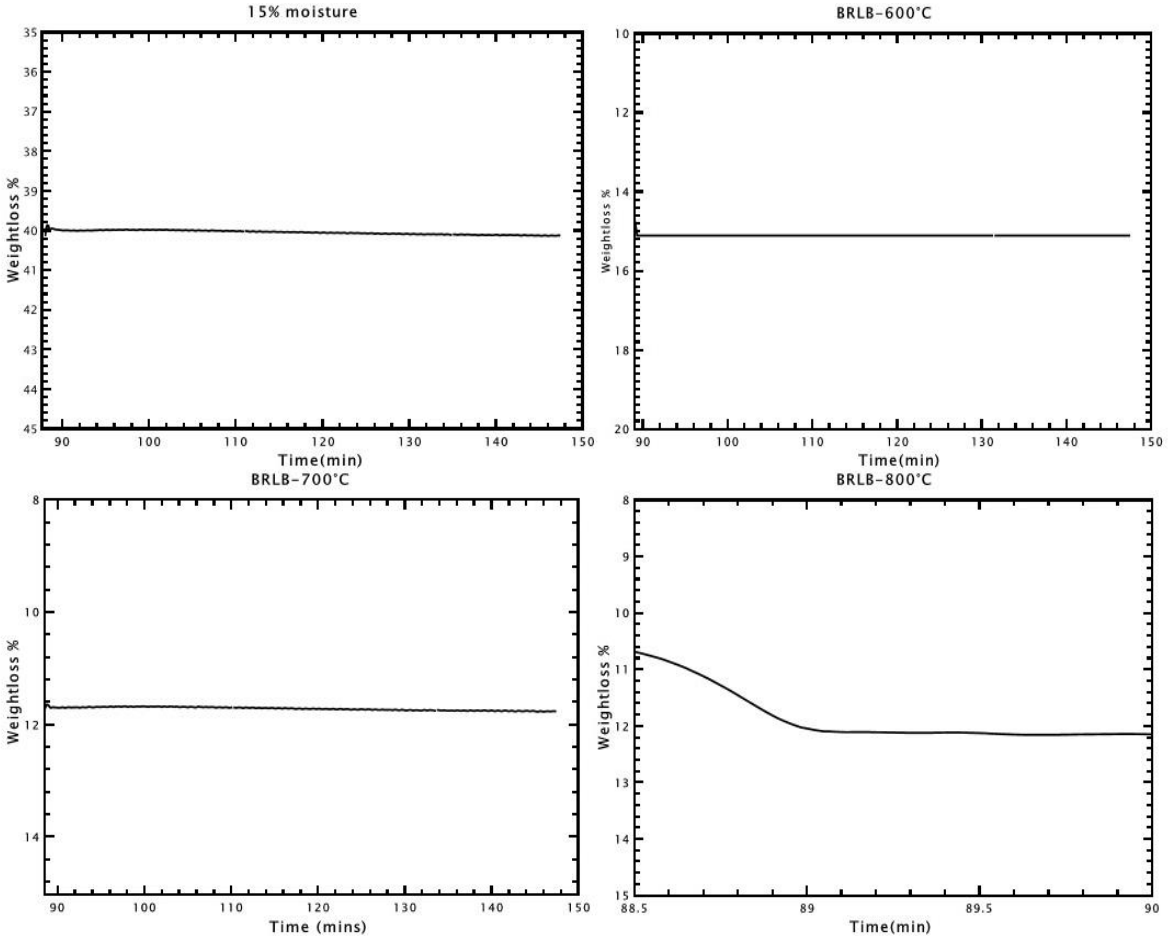

Figure 16 . Weight loss% of sludge biochar samples under synthetic air flow (25 mL/min) at 900°C

The weight loss vs time graphs show for sludge samples show a general trend of massive weight loss in less time as compared to wood. Sludge has a higher percentage of unburnt minerals and oxides that quickly react with oxygen in air and leave behind much greater ash content.

3.4 BET:

Initially wood samples were activated my heating at 250°C for three hours under vacuum before process of nitrogen sorption begin. The data was collected, graph between quantity adsorbed and relative pressure (p/p0.) were plotted on QTI plot. In all the graphs, line with solid red symbols represent quantity adsorbed of Nitrogen gas and the line with hollow red symbols shows desorption trend of nitrogen gas. Furthermore, by using equation 2 and 3 on MS Excel, monolayer adsorbed volume (Vm) and total BET surface area of the sample is calculated. Following criteria was ensured when plotting BET plots [41].

(a) the quantity C should be positive

(b) BET equations application be restricted to the range where the term n (1 – p/p0) increases with p/p0;

(c) the p/p0 value against to nm needs be within the selected BET range.:

Wood samples:

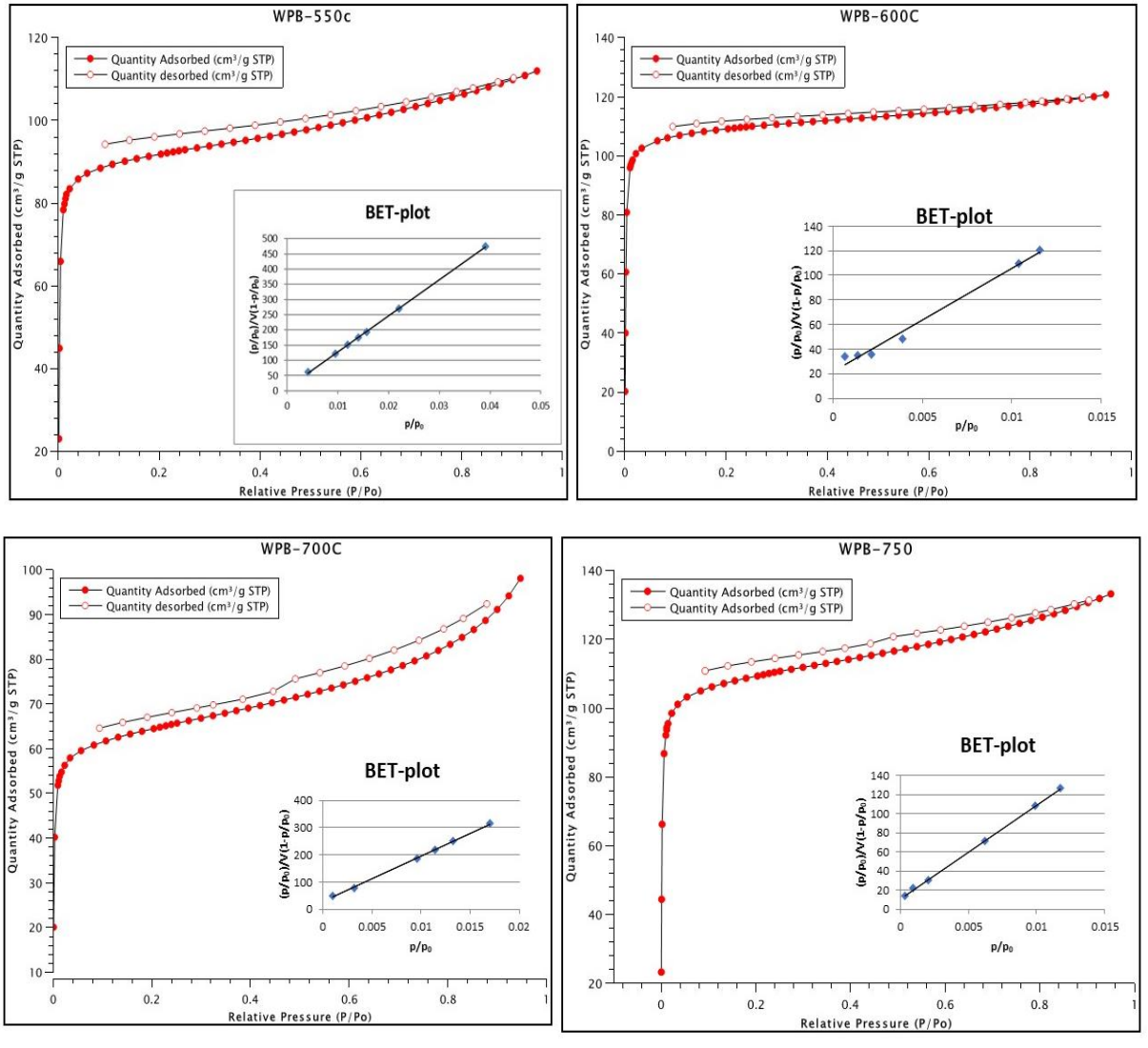

Figure 17 BET-measurement of biochar-wood samples

Figure 17 shows first two biochar samples, WPB-550°C and WPB-600°C biochar sample graphs show there is a steep uptake of nitrogen at low relative pressure of less than 0. p/p_0 (relative pressure) which is usually due to the filling of micorpore as a result of biochar and Nitrogen interaction. It is followed by slow sorptiona and the finally equillibrium stage. From orignal data, wood samples took more than 35 hours to complete the procdure and most of the time elsapsed was for less than 0.1 relative pressure p/p_0. It is almost a similar trend similar to type 1 isotherm (IUPAC) for microporous materials.

The graphs for all the samples show hysterieses of IUPAC type H4 which is usally observed in micro-mesoporous carbon, but a possible difference is that these are open loops which could be associated to pore blocking [41]. During desorption, the wide pores remain filled until narrow necks are emptied at low pressures. The desorption wood hysteresis loops remain open, which is because Nitrogen remains trapped in the pores during adsorption, which in this case can be considered as of chemisorption, which resulted in the alteration of original biochar structure.

Equation 4.2 and 4.3 were used to calculate the table 6. it can be seen that there is an increasing trend in surface area and monolayer volume and total pore volume with increasing pyrolytic temperature. This table is backed up by literature [42] as with higher pyrolysis temperature such characteristics are expected and observed. Hence, higher temperature wood samples could be idea for adsorption purposes.

Table 6 Surface area. Monolayer volume and total pore volume of wood samples

Sample	Surface area (m^2/g)	Vm (cm^3/g)	Total pore volume (cm3/g) at 0.904 p/p0	Correction coefficient
WPB- 550°C	411	94	0.156	0.994
WPB- 600°C	517	119	0.168	0.987
WPB- 700°C	546	56	0.191	0.999
WPB- 750°C	583	102	0.204	0.999

Sludge samples:

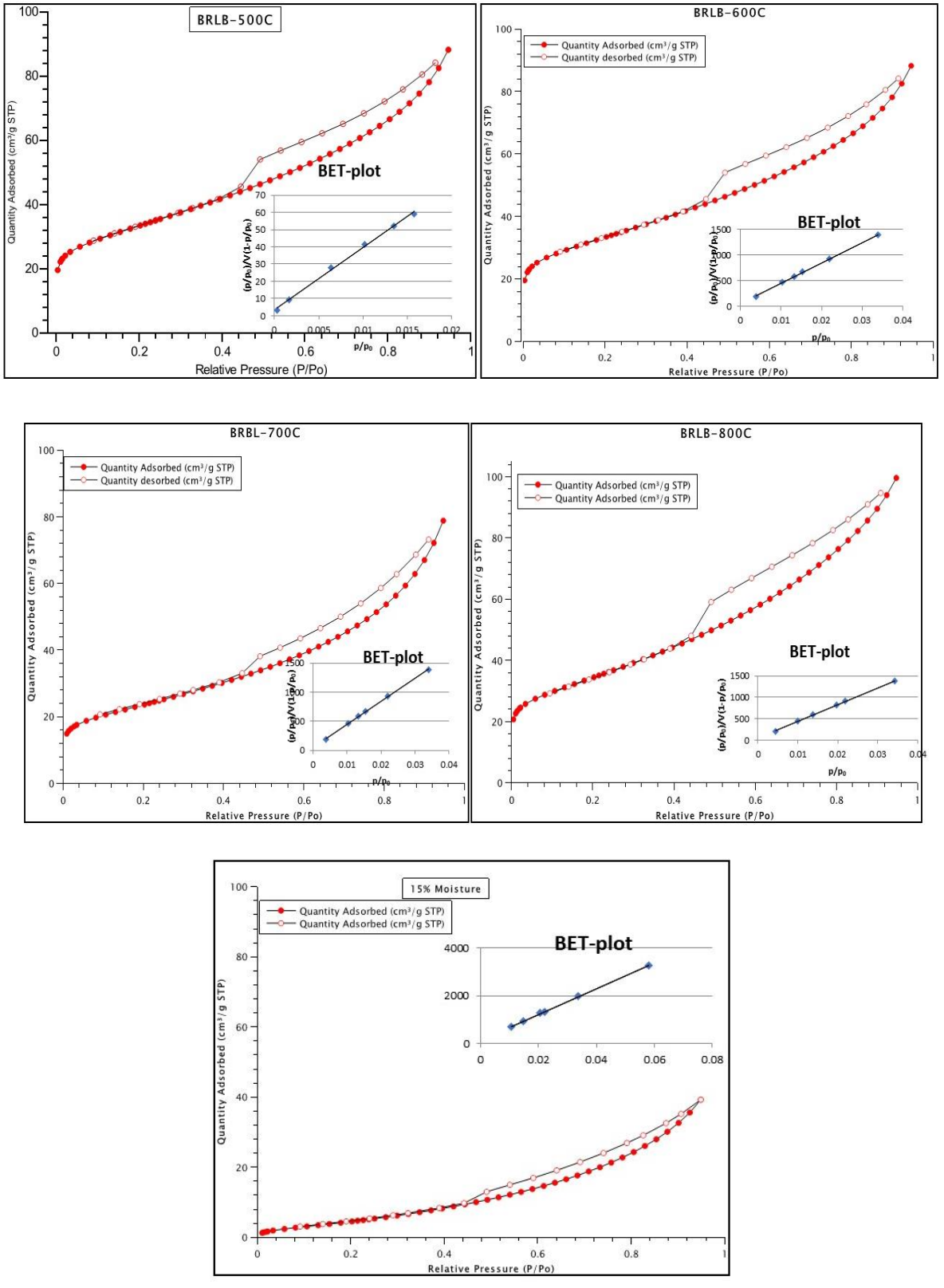

Figure 18 BET-measurement of biochar-wood samples

The graph for sludge samples shows very different shape isotherms as compared to the wood samples, according to IUPAC classification, this is reversible type 2 isotherm (Figure 18). This type of graph shows non-porous or macroporous adsorbent and of monolayer-multilayer adsorption upto high relative pressure. There is not a sharp rise in low relative pressure like wood samples, meaning absence of micropores. After a brief adsorption, at knee point graphs show a linear middle section which means complete diffusion on Nitrogen to monolayer. The absence of a strong knee point and more of a gradual curvature, means there is overlapping of monolayer coverage and beginning of multilayer adsorption. And, if we notice in the order of increasing pyrolysis temperature, there is increasing curvature in the graphs which could mean multilayer adsorption with increase in pyrolytic temperature.

There is presence of hysteresis loop on sludge samples similar to wood samples, but these are closed loop. By comparing to IUPAC classification, sludge loops are very similar to H3 kind. As the loop is closed it means no pore blocking is taking place, but there is presence of macropores in the pore network which are not completely filled with pore condensate.

Table 7 Surface area. Monolayer volume and total pore volume of sludge samples

Sample	Surface area (m^2/g)	Vm (cm^3/g)	Total pore volume (cm3/g) at 0.904 p/p0	Correction coefficient
15% Moisture	2	9	0.017	0.999
BRLB-500°C	12	27	0.055	0.994
BRLB-600°C	25	110	0.066	0.999
BRLB-700°C	80	18	0.032	0.999
BRLB-800°C	112	26	0.045	0.999

3.4.1 Pore size distribution:

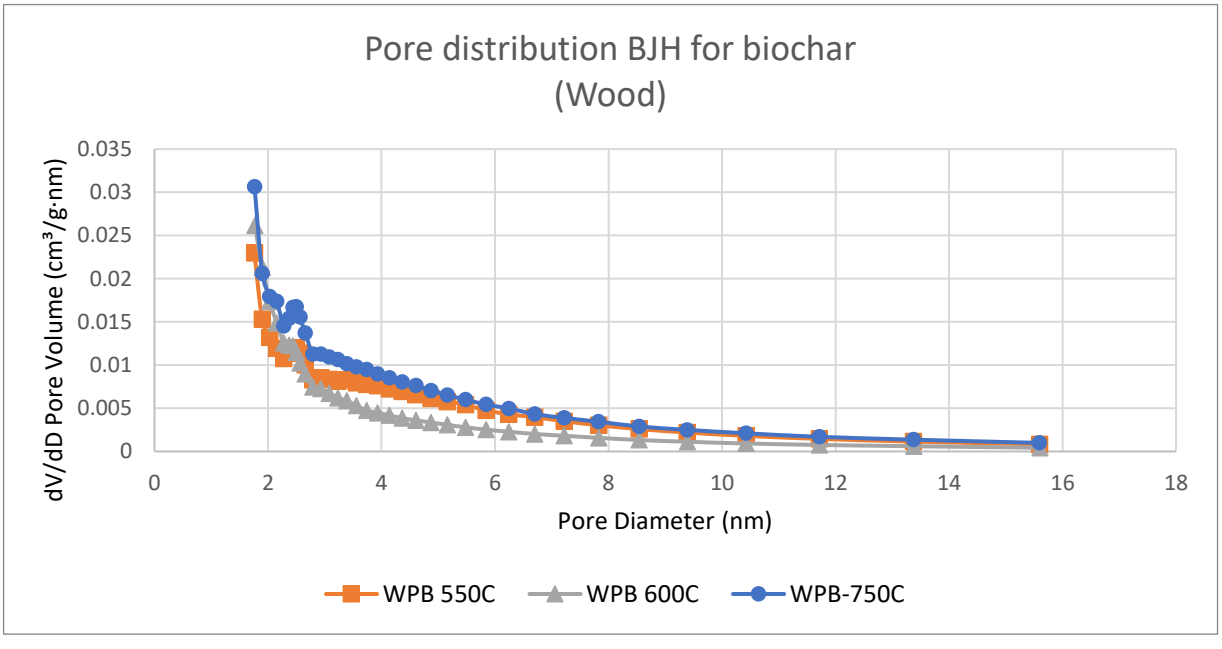

Figure 19Pore distribution BJH for wood samples at 550oc, 600oC, and 750oC

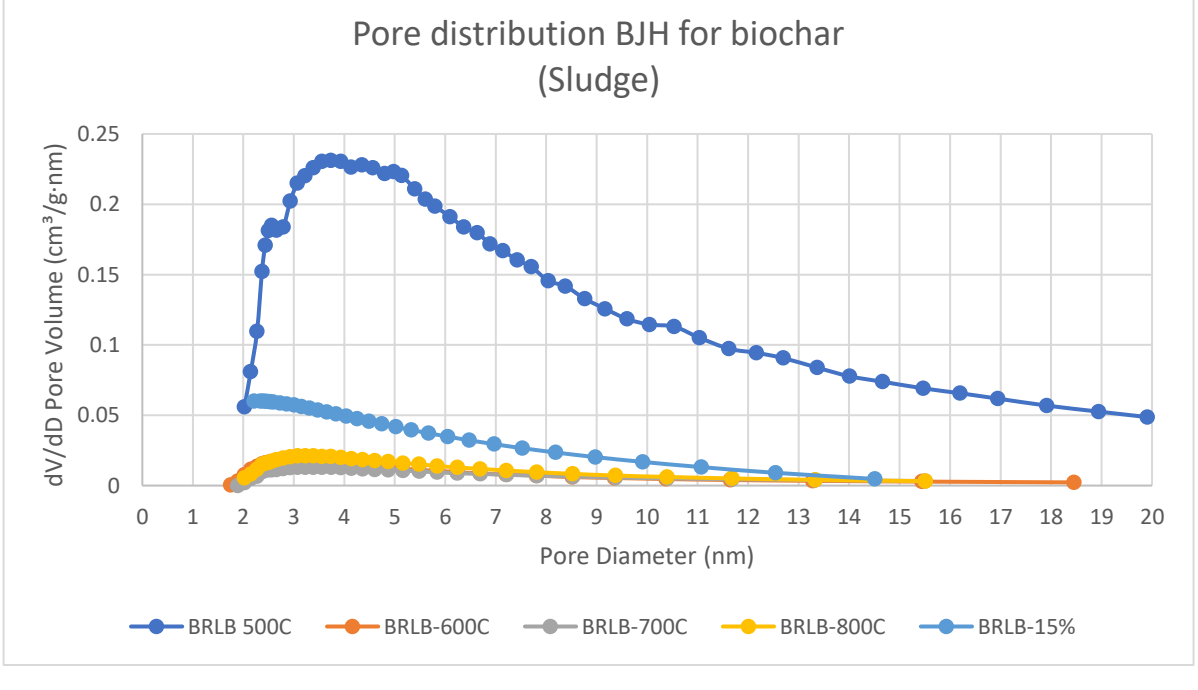

Figure 20. Pore distribution BJH for sludge samples at 550oc, 600oC, 700oC, 800oC, and 15% moisture

For pore size distribution, the classical pore size model developed by Barret, Joyner and Halenda (BJH), which is based on the Kelvin equation and corrected for multi-layer adsorption was used to plot the graphs. For wood samples figure 19, we can see that for all the samples the highest volume distribution of pores is under 2nm, the maximum peaks for WPB-750^{o}C at around 0.032cm^{3}/g·nm and decreases with pyrolytic temperature. The graph spreads till 16nm for all but most is concentrated around 2nm. Mostly pores are distributed around 2-5 nm for wood samples.

For sludge samples as shown in Figure 20, the distribution here spreads to 20nm but the volume peaks at around 4nm for BRLB 500^{o}C, and for the rest of the samples it lies around 3nm, from this data sludge samples can be categorised as mesoporous material pore distribution mostly spread between 2-7nm.

3.4.2 CO_2 adsorption

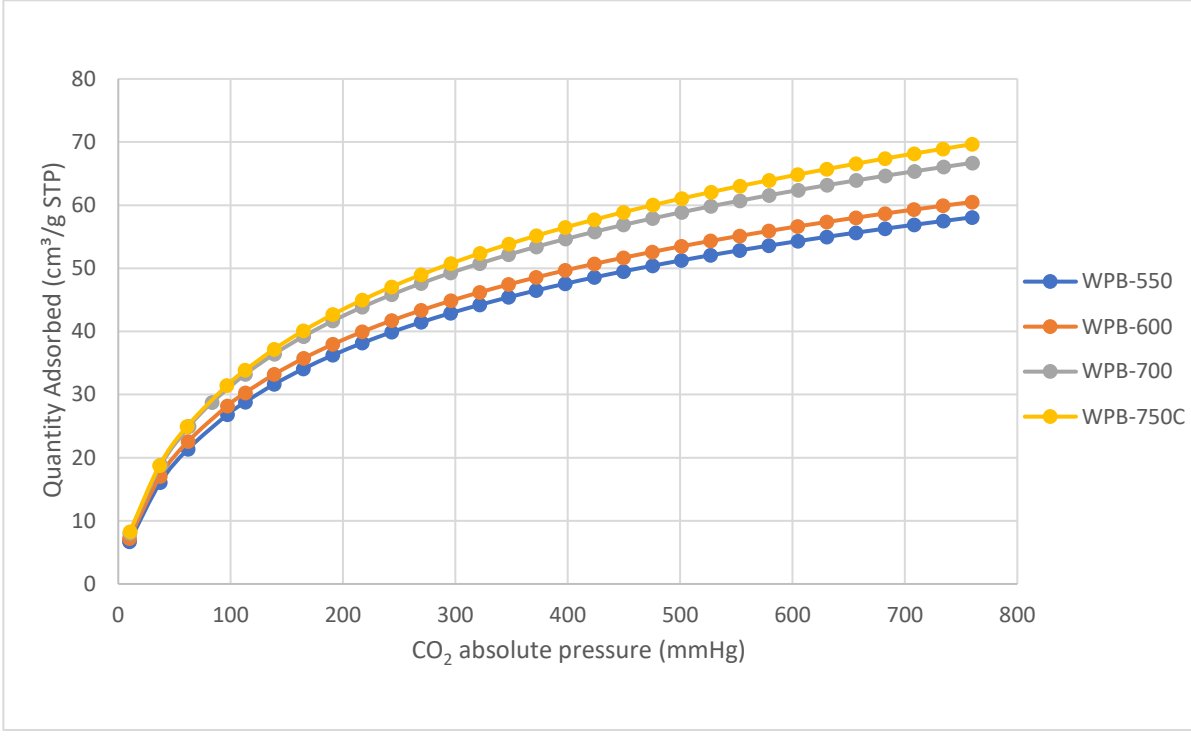

Figure 21 CO2 adsorption isotherms of wood samples

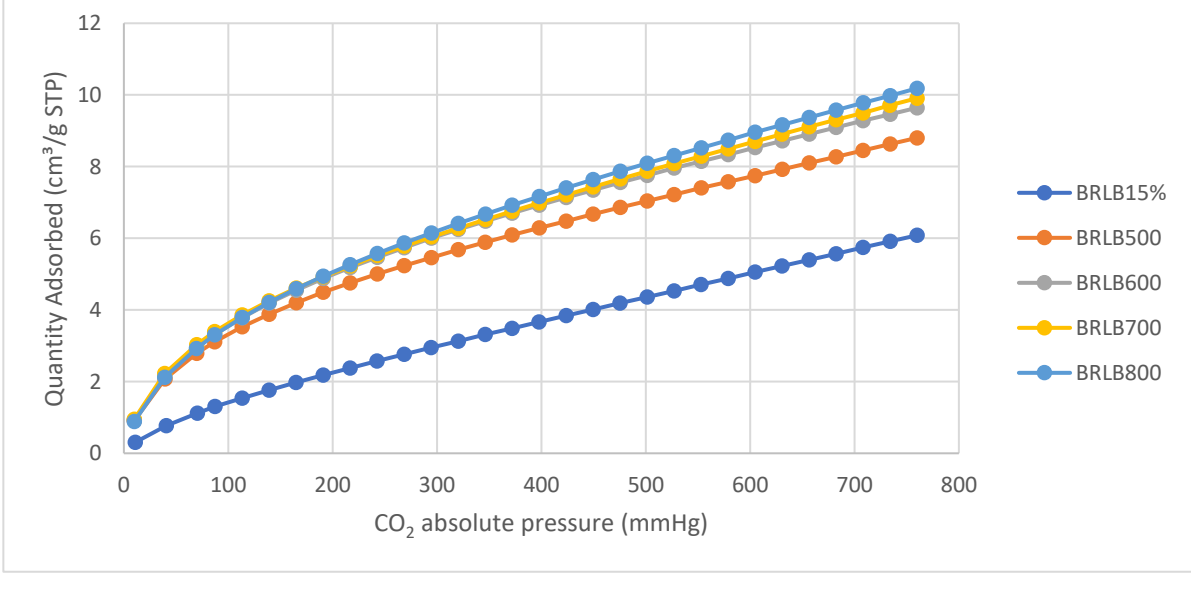

Figure 22 CO2 adsorption isotherms of sludge samples

For carboon dioxide graphs qunatity of CO_2 adsorbed was plotted against absolute pressure (Figure 21). This shows clear trent of increasing adsorption quantatity with increasing pyrlosis temperature. Wood sample of 750°C adsorbs the maximun around 70 cm³/g STP and the lowest of 550°C adsorbs around 59

cm^3/g STP. For sludge samples in figure 22, maximum adsorbed CO_2 is 11 cm^3/g STP far lower than wood sample. It further decrase down with samples of decreasing pyrolsis temperature. Since quantatity of adsorbed Nitrogen was assocated with high surface area and total pore volume , same can be concluded for CO_2 sorption.

3.4.3 Drug-uptake

3.4.3.1 Calibration *curve*

Before starting drug uptake with biochar samples, calibration curve for ciprofloxacin was plotted (Figure 24).As all the diluted solution samples were measured in UV spectrometer, the results were collected in a form of table and graphs were plotted in QtiPlot.

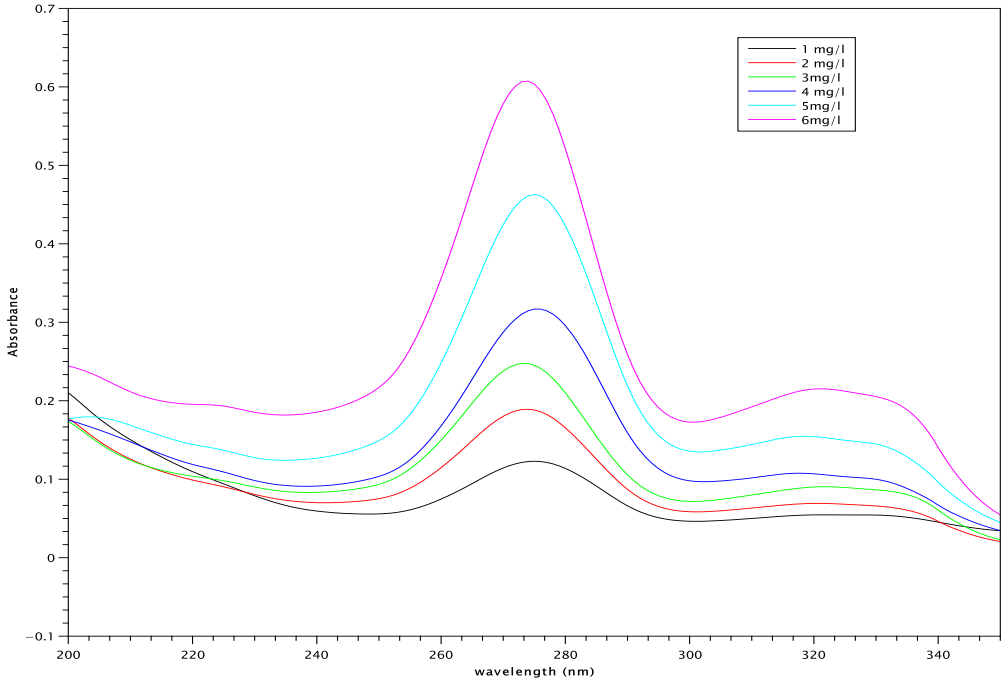

Figure 23 UV spectra of ciprofloxacin using different concentrations (1 – 6 mg/L)

Average peak can be calculated by adding each peak and dividing by number 6,

$$\text{Average} = \frac{275.0 + 274.0 + 273.0 + 276 + 275 + 274}{6}$$

$$\text{Average} = 274.5\text{nm}$$

For further drawing the calibration curve, linear approximation of absorbance from our data at of different concentrations at average wavelength of 274.5nm. The data was used to plot the calibration curve in Microsoft Excel, line of best fit was drawn, and equation of line was also determined.

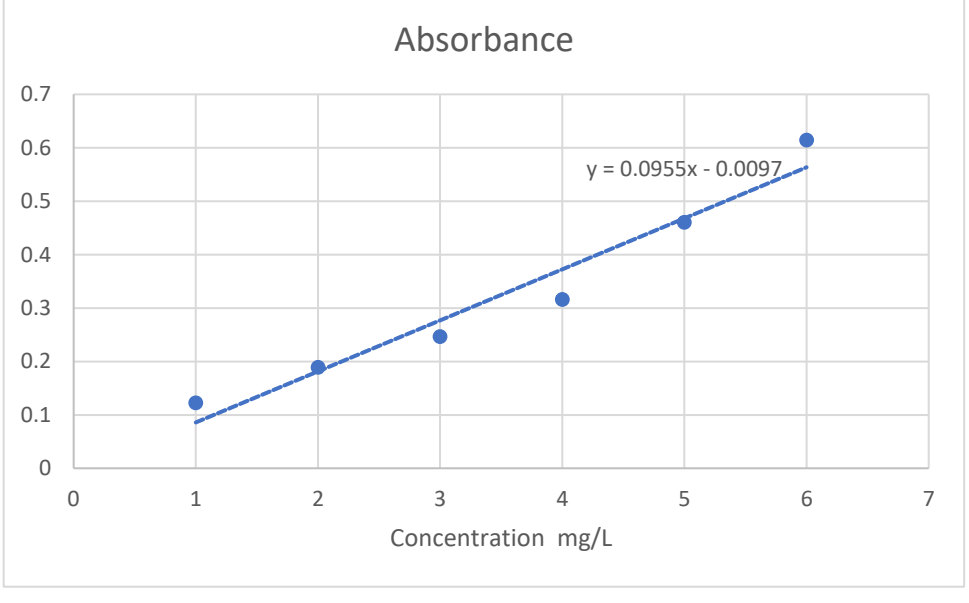

figure 24 Calibration curve of ciprofloxacin

Further to check derivation in measurement of UV spectra, three sample solutions of lowest and highest concentration solution, 1mg/l and 6mg/l were measured and graphs plotted.

3.4.3.2 Low concentration solutions

As there were in total three samples made for the lowest and highest concentration 1 mg/L and 6mg/L, the solutions were tested, and the Spectra was obtained, and the following graphs were seen.

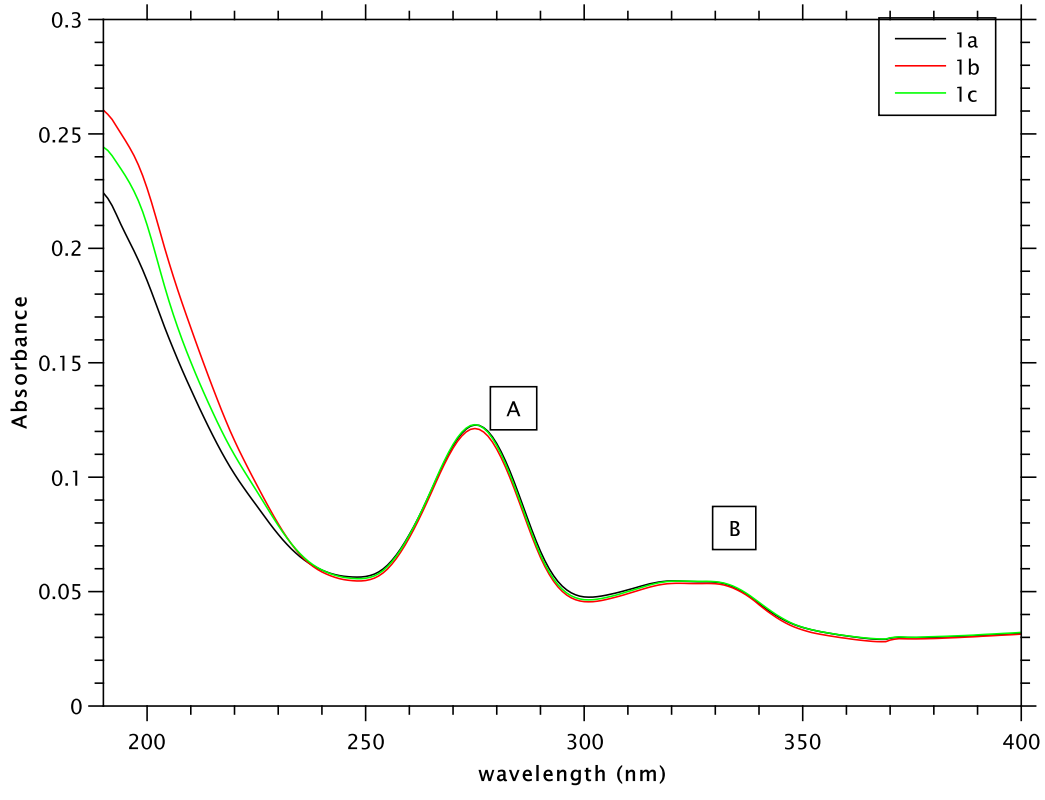

Figure 25 UV spectra of 1mg/L, thrice spectra measurement

Table 8 Standard deviation measurements in 3 samples of 1mg/L solutions

Solutions	Peak A(275)	Mean ($\bar{x}$)	σ	σ^2	$\Sigma \sigma^2$
1mg/L a	0.122808	0.122335	4.73×10^{-4}	2.23×10^{-4}	2.24×10^{-4}
1mg/L b	0.121260	0.122335	1.08×10^{-3}	1.16×10^{-6}	
1mg/L c	0.122938	0.122335	6.03×10^{-4}	3.64×10^{-7}	

Variance= $\Sigma \frac{\sigma 2}{} n - 1$

Variance =2.24x10^{-4}/2

Variance= 1.122 x 10^{-4}

Standard deviation= √1.122 x 10^{-4}

Standard deviation=0.0106

From the data it can be seen that there were 2 peaks observed because of Ciprofloxacin A and B, both are because of Ciprofloxacin, they appear differently because of different bonding mechanisms, The absorbance of three similar concentration solutions 1 mg/l is slightly different, so standard derivation was calculated and, in the chart, it is seen them from mean value.

3.4.3.3 High concentration solutions:

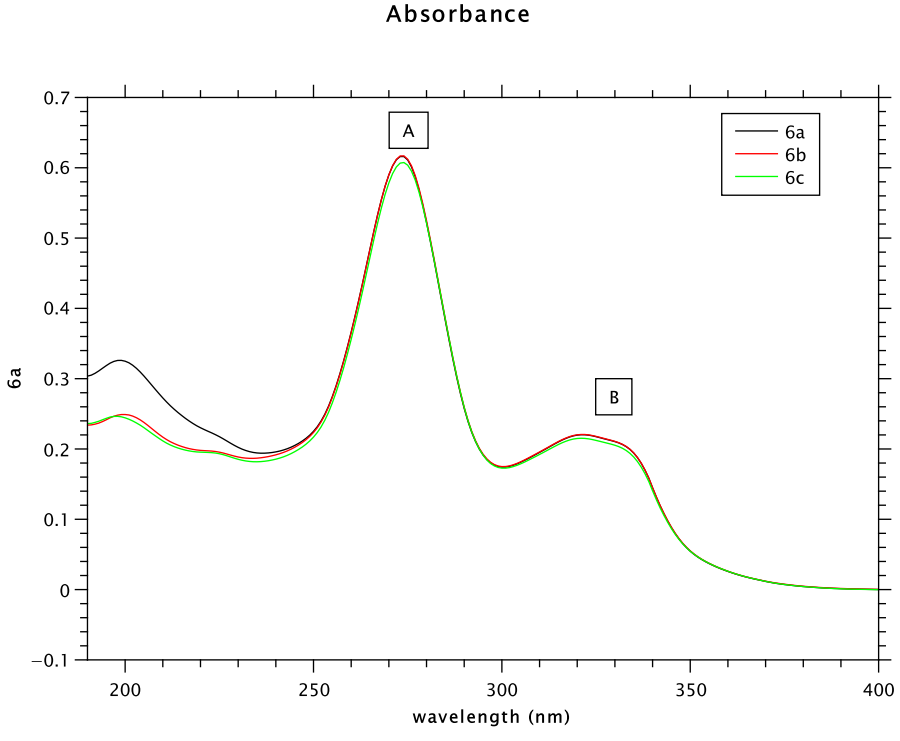

Figure 26 UV spectra of 3 different samples of 6mg/L spectra

Table 9 standard deviation measurements in 3 samples of 6mg/L solutions

Solutions	**Peak A(275)**	**Mean ($\bar{x}$)**	**σ**	**σ^2**	**Σ σ^2**
6mg/L a	0.611064	0.611788	$7.24x\ 10^{-4}$	$5.24x10^{-7}$	$4.53x10^{-5}$
6mg/L b	0.616872	0.611788	$5.08\ x\ 10^{-3}$	$2.58x10^{-5}$	
6mg/L c	0.607428	0.611788	$4.36x10^{-3}$	$1.90x10^{-5}$	

Variance= $\Sigma\ \sigma^2/n - 1$

Variance $=4.53x10^{-5}/2$

Variance= $2.67\ x\ 10^{-5}$

Standard deviation= $\sqrt{2.67\ x\ 10^{-5}}$

Standard deviation=$4.76\ 10^{-3}$

In second experiment, solutions with the lowest and highest concentrations, 1mg/L and 6mg/L what are measured three times for UV spectrometry. The reserves from the graph indicate that at the wavelength of 274 the absorbance was 100% similar in both the cases. Since there were no differences in the absorbance reading so calculations for standard deviations were not performed.

3.4.4 Ciprofloxacin and Sludge biochar:

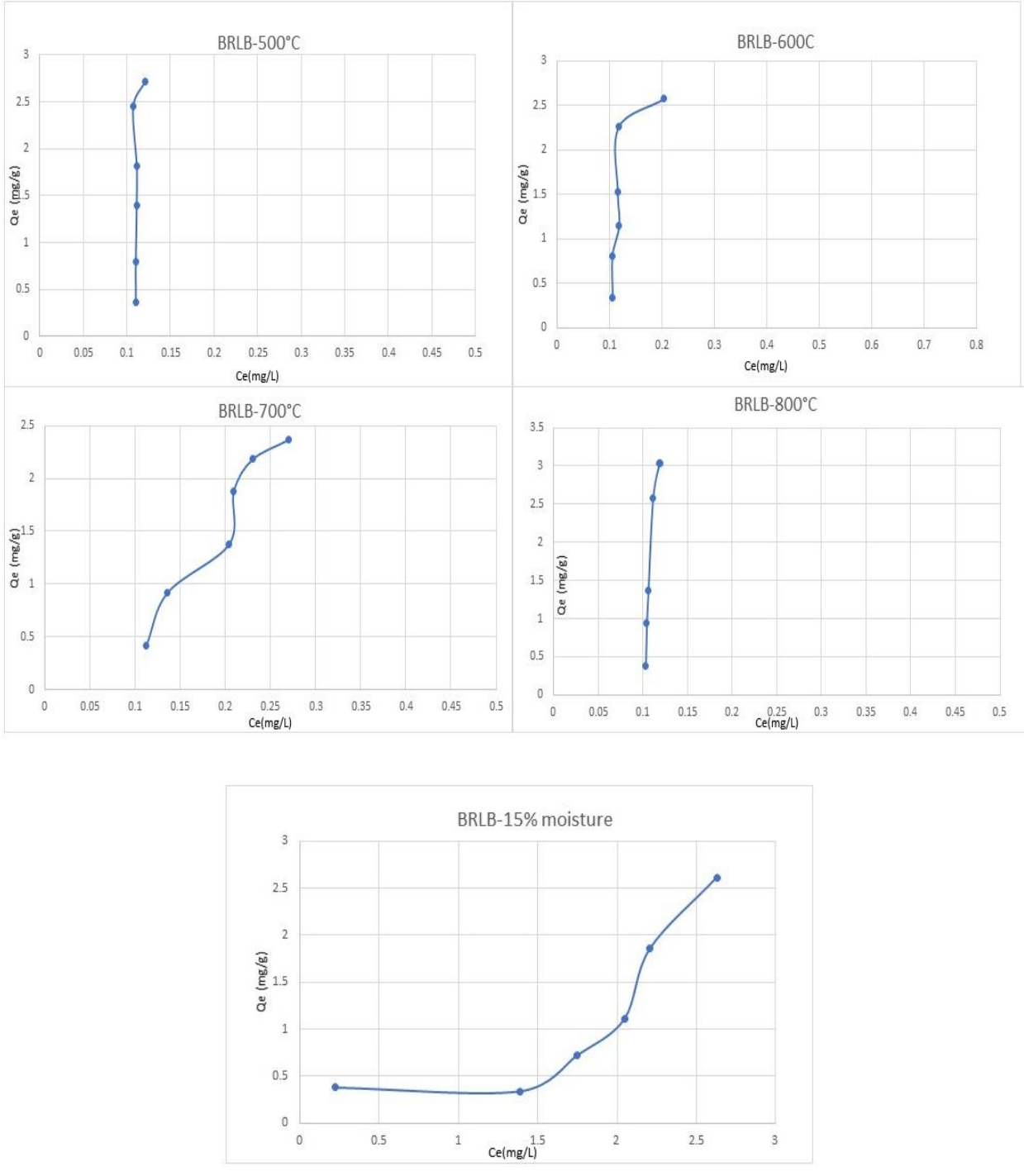

Figure 27 Adsorption isotherm models of ciprofloxacin on the sludge biochar samples

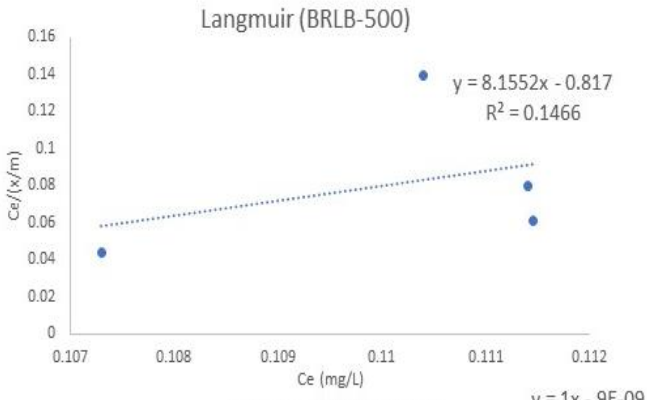
Langmuir (BRLB-500)
y = 8.1552x - 0.817
R² = 0.1466
Ce/(x/m)
Ce (mg/L)

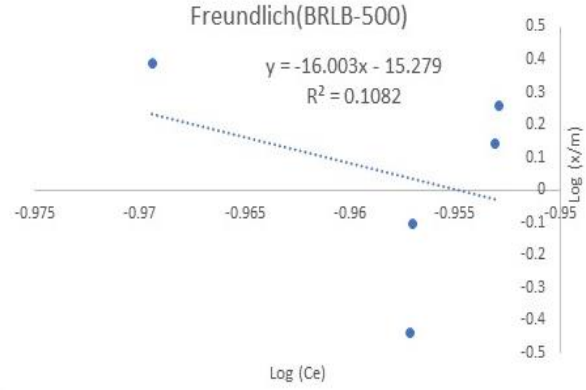
Freundlich(BRLB-500)
y = -16.003x - 15.279
R² = 0.1082
Log (x/m)
Log (Ce)

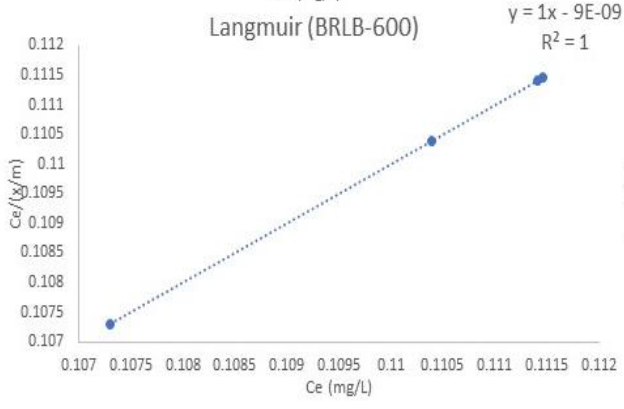
Langmuir (BRLB-600)
y = 1x - 9E-09
R² = 1
Ce/(x/m)
Ce (mg/L)

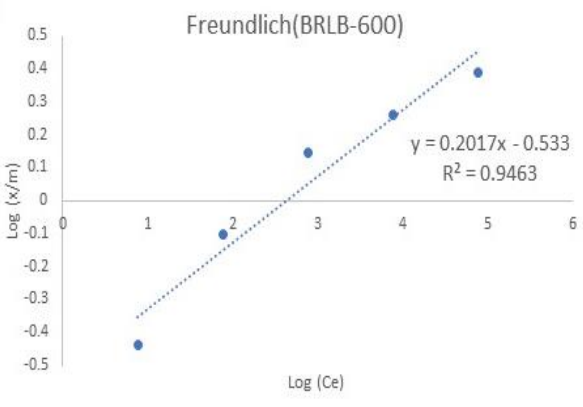
Freundlich(BRLB-600)
y = 0.2017x - 0.533
R² = 0.9463
Log (x/m)
Log (Ce)

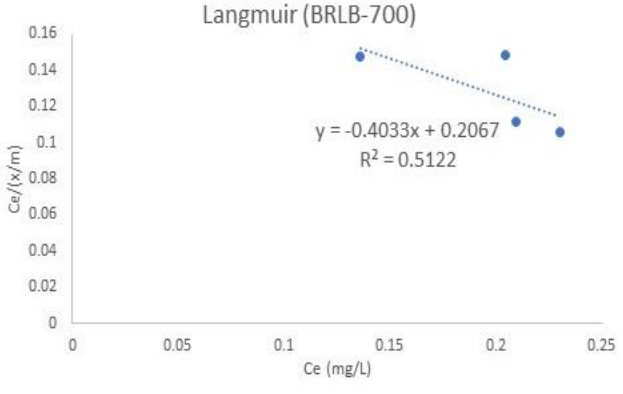
Langmuir (BRLB-700)
y = -0.4033x + 0.2067
R² = 0.5122
Ce/(x/m)
Ce (mg/L)

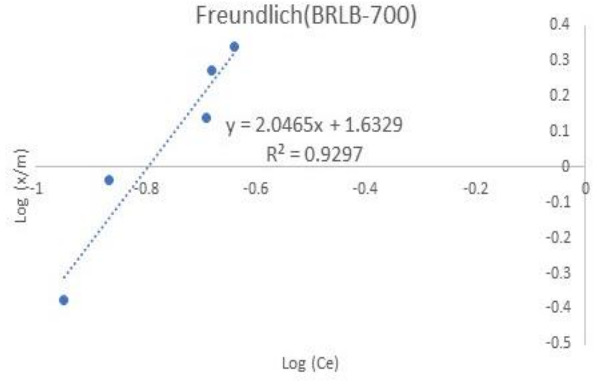
Freundlich(BRLB-700)
y = 2.0465x + 1.6329
R² = 0.9297
Log (x/m)
Log (Ce)

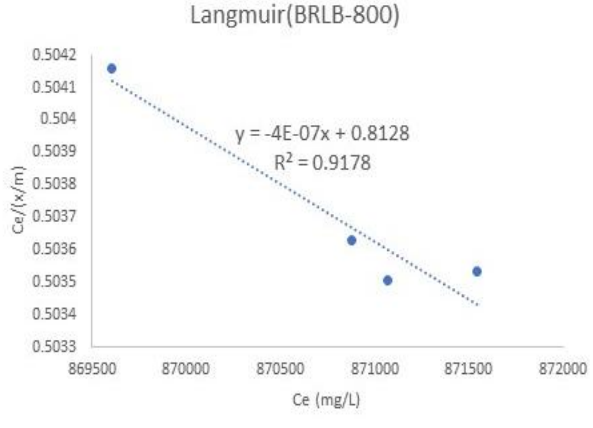
Langmuir(BRLB-800)
y = -4E-07x + 0.8128
R² = 0.9178
Ce/(x/m)
Ce (mg/L)

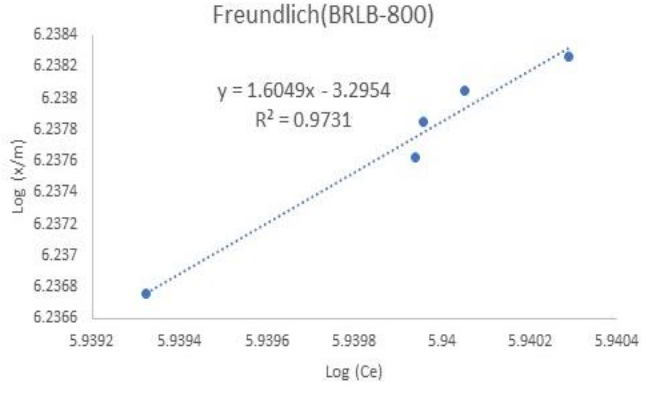
Freundlich(BRLB-800)
y = 1.6049x - 3.2954
R² = 0.9731
Log (x/m)
Log (Ce)

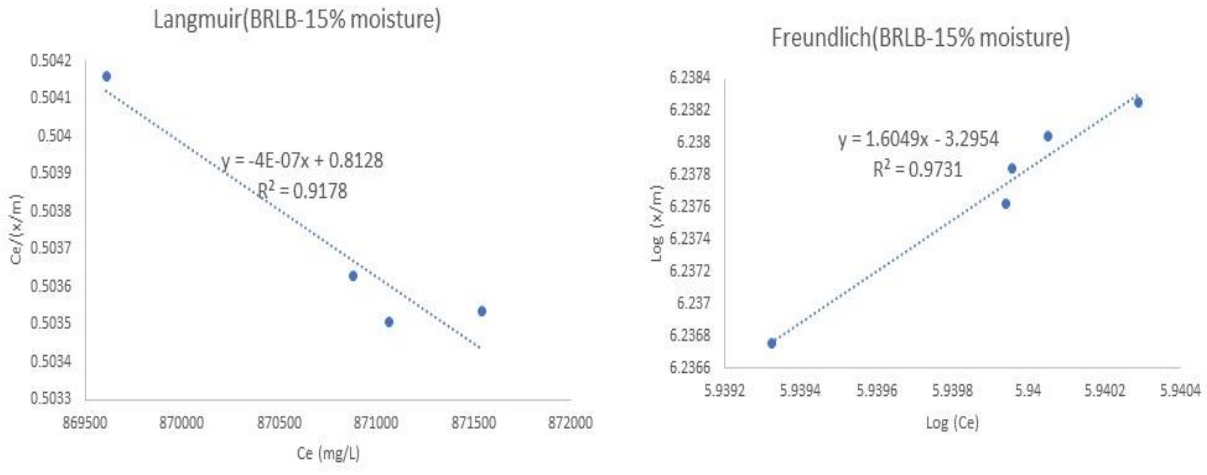

Figure 28 Langmuir and Freundlich models for sludge samples plotted from equation 7 and equation 8

Adsorption isotherms using sludge biochar show a general trend of adsorption increasing efficiency of biochar, it shows that the adsorbed quantity increases as a function of the equilibrium concentration and expected to increase until saturation with a maximum adsorbed quantity, which in this case has not reached and if tested with higher concentrations is expected to reach saturation point (Figure 27). If we look at graphs with increasing pyrolytic temperature, we see that adsorption capacity increases with increasing temperature. For examples for sludge of 500°C Qe value is around 2.6mg/g and for 800°C it is 3.1mg/g.

Furthermore, Langmuir and Freundlich models [43] were used to study the correlation between the amount of adsorbed ciprofloxacin and the equilibrium concentration. Four data points and equation 5 and 6 were used to plot the line of best fit. From the graphs (Figure 27), the correlation coefficients, R^2 for both the models for sludge-500°C sample is very low, less than 0.90 as the models do not show high relevance with experimental data, other models need to be checked and more experimental data points are required for better results. Langmuir model describes the monolayered adsorbents on the homogeneous surface [44]. For, BRLB-600°C Langmuir models (R^2=0.9463) fit better indicating that specific homogenous sites within the adsorbent are involved. For BRLB-700, 800 and unprocessed sludge samples; shows some difference between Langmuir and Freundlich isotherm model fit which could suggest that there is highly heterogeneous distribution of sorption energy and existence of the intermolecular interactions that occur between ciprofloxacin and biochar.

With increasing pyrolysis temperature, the trend is not as expected in the literature [45], as sample 600°C and 700°C show lower adsorbent capacity than sample with 500°C. this could be because of highly variable composition of sludge, as it sources, and processing cannot always be the same. The

mass used for adsorbent could be a factor that might have affected its performance as 0.50 mg was used for all samples but heating to remove moisture leaves less and different amount of biochar behind and further concentration of ciprofloxacin used could be very low and can go undetected by UV, in that case different methodology needs to be adopted.

Experiments with sludge and biochar samples had to performed multiple times to reach consistent results with literature. Repetition was done to eliminate experimental or instrumental errors. Due to limited Master's thesis time and period, results could not be produced multiple times, with changing variables to produce the most ideal results.

3.4.5 Ciprofloxacin and wood biochar:

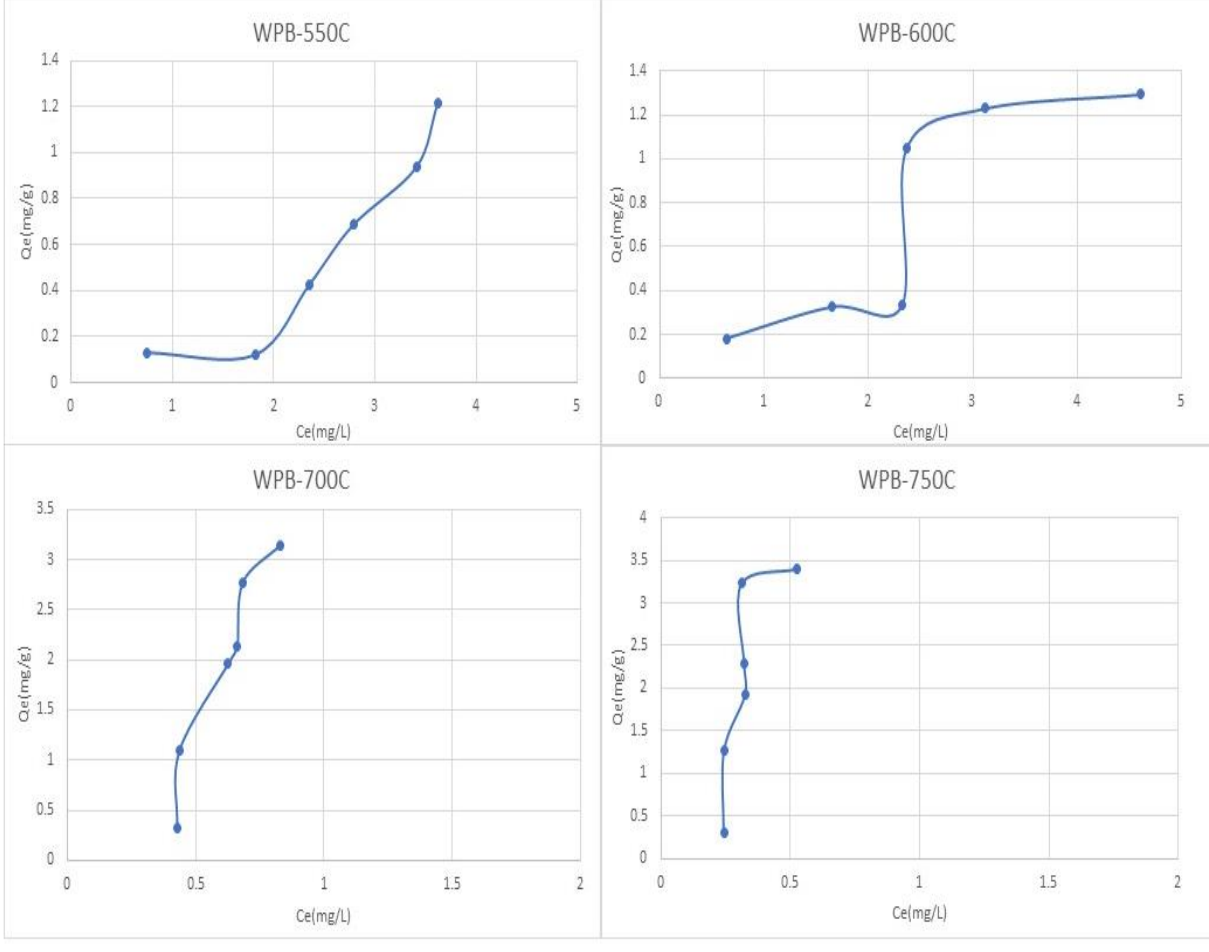

Figure 29 . Adsorption isotherm models of ciprofloxacin on the wood biochar samples

Wood samples show much promising result as samples adsorption capacity gradually increases with pyrolysis temeprature which is very consistent with BET surafce area. But it is noted that difference of 50°C between samples donnot show as much of a difference as 100°C show. Qe value increases from

1.2mg/g of WPB-550 to 3.4mg/g for WPB-750°C. For most of samples the isotherms donot biochar have reached saturation that means batch experiments with higher concentration and higher differnece bewteen the concentrations need to be performed.

Similarly here two models Langmuir and Freundlich [46] were used to be fitted to experiment data (Fig. 31). In several studies of biochar adsorption, Langmuir model was best fitted [47]. However, in this data, Langmuir model was not fitted As shown in Fig. 32, Freundlich model for WPB-550°C and WPB-750°C with R^2 values of 0.9515 and 0.9513 well-fitted this model indicated that the adsorption would take place with a heterogeneous surface.But for WPB-600°C and WPB-700°C, non of the models fit. Other models could bb checked and plotted with more data points and changing varaibles.

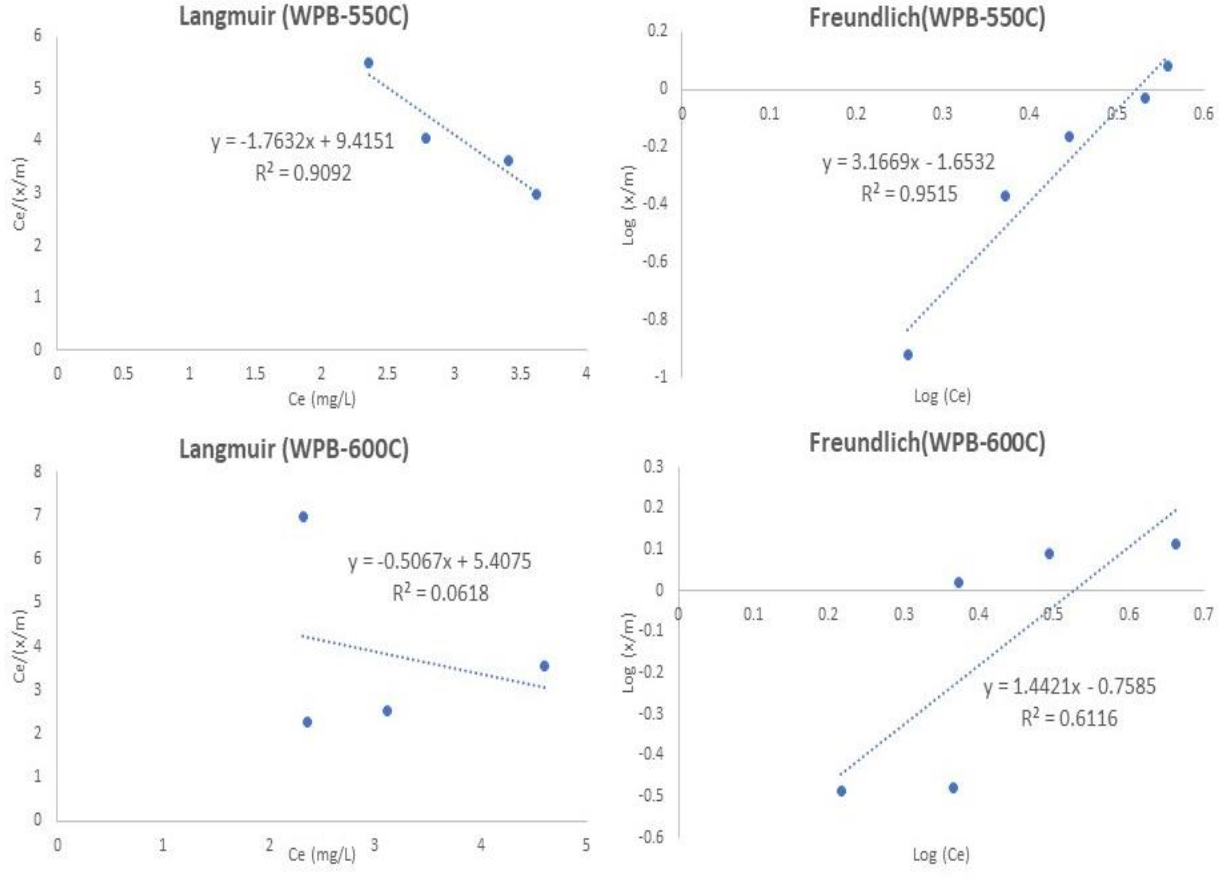

Figure 30 Langmuir and Freundlich linear isotherm plot for WPB-550 and WPB-600 plotted from equation 7 and equation 8

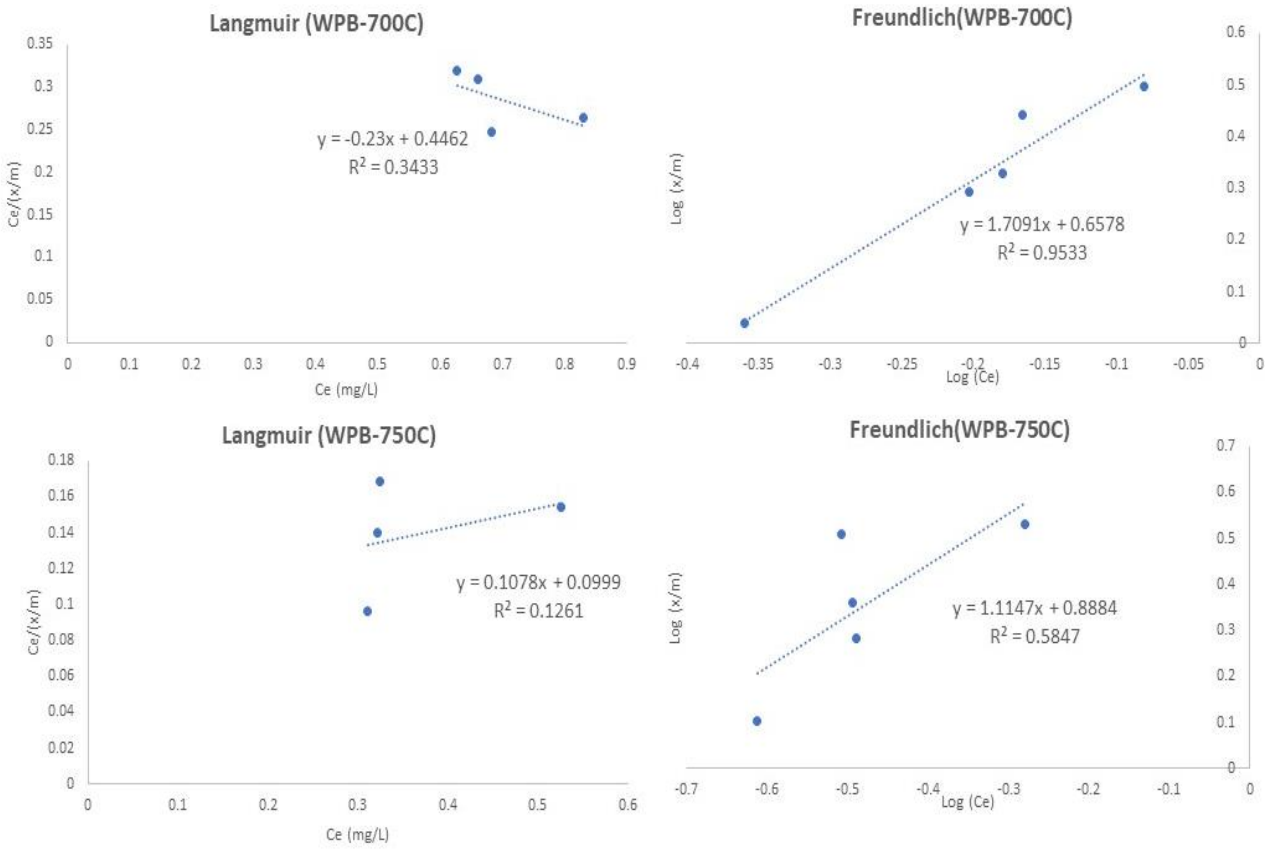

Figure 31 Langmuir and Freundlich linear isotherm plot for WPB-550 and WPB-600

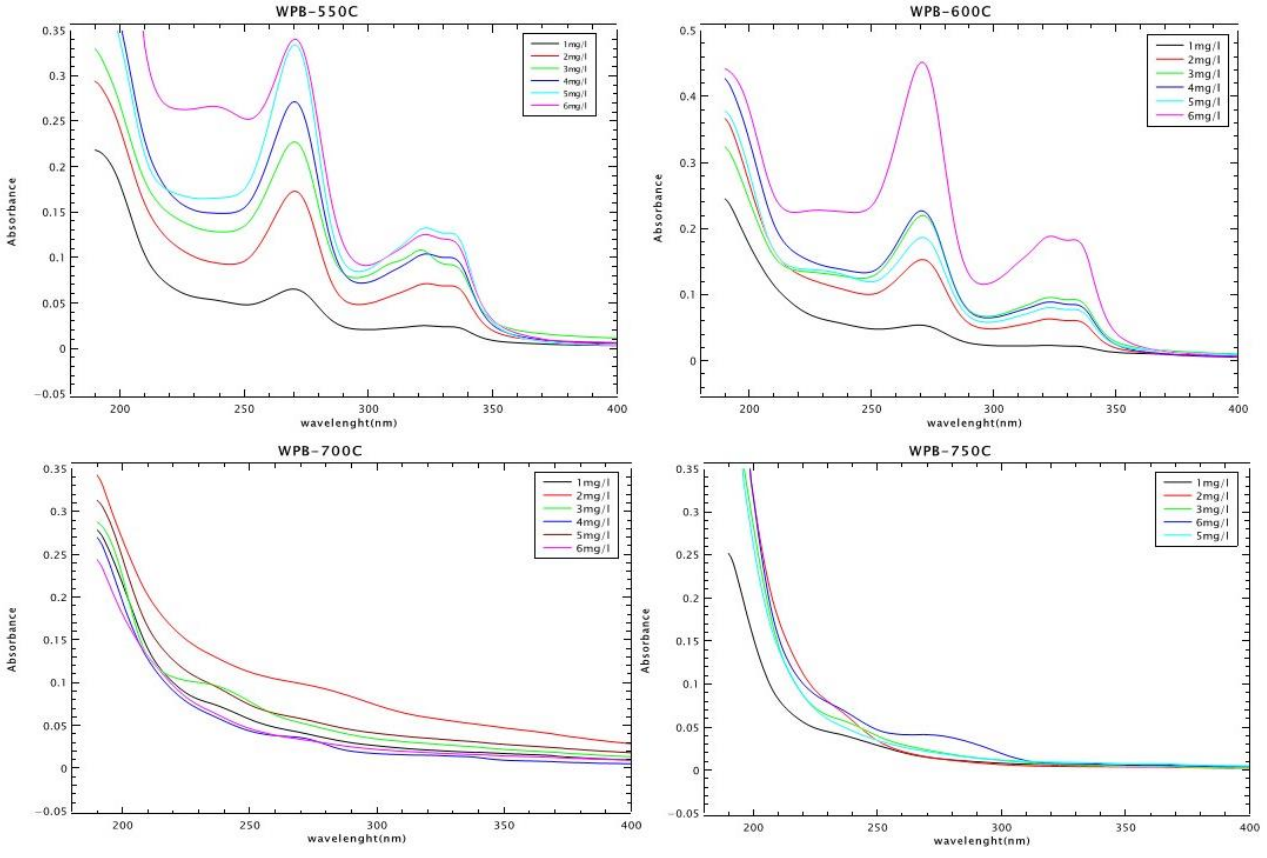

Figure 32 UV spectra for wood samples

4 Conclusion

Ciprofloxacin has various sources of entering the environment like pharmaceutical industrial, human, and veterinary hospitals wastes. Studies have shown it has irreversible effects on local ecology, environment and human health and the problem is only expected to increase in future. This study was aimed at reviewing ciprofloxacin as a pollutant and biochar as an adsorbent to remove ciprofloxacin from wastewater. Current WWTP are not designed to treat such amounts of pharmaceuticals and treating it at the source before it enters the environment could be a smart way to eliminate. Biochar was received from Scanship AS, which originates from two sources wood and sludge, pyrolyzed at different temperature between 500°C and 800°C along with un-pyrolyzed sludge sample to compare results with. Different characterisation techniques were used to find out its efficiency and possible behaviour as an adsorbent and it showed promising results. XRD was performed and it showed biochar has high degree of amorphous and it increases with pyrolysis temperature, the behaviours were better in woods samples than sludge samples. ATR-FTIR was performed to find out functional groups in biochar samples, it showed -OH and other carbon groups for sludge samples but was not very helpful for wood samples and it is suggested to use NMR, pyrolysis GC-MS or high-resolution mass spectrometry in further studies as these have higher sensitivity to species present in biochar. As TGA was performed that concluded wood samples have lower moisture content than sludge samples and decreased with temperature and wood biochar had very low ash content whereas sludge sample consisted of 60-80% ash content due to low carbon and high mineralisation. BET showed increasing surface area and microporosity and total pore volume with temperature for both types of biochar, but sludge samples had much lower values especially microporosity and surface area meaning wood sample have better abilities for adsorption purpose. Finally, drug uptake was performed and similarly wood samples with higher temperature proved to have better adsorption capacity as compared to sludge samples but less than shown in literature, but this is not conclusive as isotherms need to have reached saturation point which need additional data points of higher than 6mg/l of initial CIP. Furthermore, batch experiments need to be performed with variable adsorbent doses, temperature and other factors and reaction kinetics need to be viewed, HPLC is recommended to be used as smaller concentrations may get unobserved by UV spectroscopy. Biochar has also shown some tricky behaviour and for further studies should use elementary analysis and SEM to better understand characteristics of biochar samples like sludge that have very variable feedstock composition.

5 References

1. aus der Beek, T., et al., *Pharmaceuticals in the environment—Global occurrences and perspectives.* Environmental toxicology and chemistry, 2016. **35**(4): p. 823-835.
2. Berglund, B., et al., *Efficient removal of antibiotics in surface-flow constructed wetlands, with no observed impact on antibiotic resistance genes.* Science of the total environment, 2014. **476**: p. 29-37.
3. Harvey, P.R., et al., *Incidence, morbidity and mortality of patients with achalasia in England: findings from a study of nationwide hospital and primary care data.* Gut, 2019. **68**(5): p. 790-795.
4. *Pubchem*. Available from: https://pubchem.ncbi.nlm.nih.gov/compound/Ciprofloxacin.
5. Kurasam, J., et al., *Presence of fluoroquinolone resistance with persistent occurrence of gyrA gene mutations in a municipal wastewater treatment plant in India.* Chemosphere, 2018. **211**: p. 817-825.
6. Kamarudheen, N., T. Naushad, and K.V.B. Rao, *Biosynthesis, characterization and antagonistic applications of extracellular melanin pigment from marine Nocardiopsis Sps.* Ind. J. Pharm. Educ. Res, 2019. **53**: p. 112-120.
7. Ahmed, M.B., et al., *Progress in the preparation and application of modified biochar for improved contaminant removal from water and wastewater.* Bioresource technology, 2016. **214**: p. 836-851.
8. Rajapaksha, A.U., et al., *Engineered/designer biochar for contaminant removal/immobilization from soil and water: potential and implication of biochar modification.* Chemosphere, 2016. **148**: p. 276-291.
9. Liu, X., et al., *Biosorption of copper ions from aqueous solution using rape straw powders: optimization, equilibrium and kinetic studies.* Ecotoxicology and Environmental Safety, 2018. **150**: p. 251-259.
10. Duan, Y., et al., *Pollution control in biochar-driven clean composting: Emphasize on heavy metal passivation and gaseous emissions mitigation.* Journal of Hazardous Materials, 2021. **420**: p. 126635.
11. Zhao, F., et al., *Bioaccumulation of antibiotics in crops under long-term manure application: Occurrence, biomass response and human exposure.* Chemosphere, 2019. **219**: p. 882-895.
12. Thomas, K.V., et al., *Source to sink tracking of selected human pharmaceuticals from two Oslo city hospitals and a wastewater treatment works.* Journal of Environmental Monitoring, 2007. **9**(12): p. 1410-1418.
13. Musarurwa, H. and N.T. Tavengwa, *Application of carboxymethyl polysaccharides as bio-sorbents for the sequestration of heavy metals in aquatic environments.* Carbohydrate polymers, 2020. **237**: p. 116142.
14. Sadeghi, M., *Synthesis of a biocopolymer carrageenan-g-poly (AAm-co-IA)/montmorilonite superabsorbent hydrogel composite.* Brazilian Journal of Chemical Engineering, 2012. **29**(2): p. 295-305.
15. Wang, Y.-Y., et al., *Attenuated total reflection-Fourier transform infrared spectroscopy (ATR-FTIR) combined with chemometrics methods for the classification of Lingzhi species.* Molecules, 2019. **24**(12): p. 2210.
16. Ropelewska, E., *Post-harvest assessment of wheat and barley kernel infections with fungi of the genus Fusarium using thermal analysis.* Journal of Stored Products Research, 2019. **83**: p. 61-65.
17. Chang, Y.-C., et al., *Anodic performances of mesocarbon microbeads (MCMB) prepared from synthetic naphthalene isotropic pitch.* Carbon, 1999. **37**(8): p. 1285-1297.

18. Naderi, M., *Surface area: brunauer–emmett–teller (BET)*, in *Progress in filtration and separation*. 2015, Elsevier. p. 585-608.
19. Thommes, M., *Textural characterization of zeolites and ordered mesoporous materials by physical adsorption.* Studies in surface science and catalysis, 2007: p. 495-523.
20. Donohue, M. and G. Aranovich, *Classification of Gibbs adsorption isotherms.* Advances in colloid and interface science, 1998. **76**: p. 137-152.
21. Mukhtar, A., et al., *Extension of BET theory to CO2 adsorption isotherms for ultra-microporosity of covalent organic polymers.* SN Applied Sciences, 2020. **2**(7): p. 1-4.
22. *Visible and Ultraviolet Spectroscopy*. Available from: https://www2.chemistry.msu.edu/faculty/reusch/virttxtjml/spectrpy/uv-vis/spectrum.htm.
23. Shaaban, A., et al., *Influence of heating temperature and holding time on biochars derived from rubber wood sawdust via slow pyrolysis.* Journal of Analytical and Applied Pyrolysis, 2014. **107**: p. 31-39.
24. Shaaban, A., et al., *Characterization of biochar derived from rubber wood sawdust through slow pyrolysis on surface porosities and functional groups.* Procedia Engineering, 2013. **68**: p. 365-371.
25. Chowdhury, Z.Z., et al., *Influence of carbonization temperature on physicochemical properties of biochar derived from slow pyrolysis of durian wood (Durio zibethinus) sawdust.* BioResources, 2016. **11**(2): p. 3356-3372.
26. Clemente, J.S., et al., *Differentiating inorganics in biochars produced at commercial scale using principal component analysis.* ACS omega, 2018. **3**(6): p. 6931-6944.
27. Takagi, H., et al., *XRD analysis of carbon stacking structure in coal during heat treatment.* Fuel, 2004. **83**(17-18): p. 2427-2433.
28. Behazin, E., et al., *Mechanical, chemical, and physical properties of wood and perennial grass biochars for possible composite application.* BioResources, 2016. **11**(1): p. 1334-1348.
29. Liu, Y., et al., *Characterization of bio-char from pyrolysis of wheat straw and its evaluation on methylene blue adsorption.* Desalination and Water Treatment, 2012. **46**(1-3): p. 115-123.
30. Waqas, M., et al., *Development of biochar as fuel and catalyst in energy recovery technologies.* Journal of cleaner production, 2018. **188**: p. 477-488.
31. Naeem, M.A., et al., *Batch and column scale removal of cadmium from water using raw and acid activated wheat straw biochar.* Water, 2019. **11**(7): p. 1438.
32. Singh, V. and V.C. Srivastava, *Self-engineered iron oxide nanoparticle incorporated on mesoporous biochar derived from textile mill sludge for the removal of an emerging pharmaceutical pollutant.* Environmental Pollution, 2020. **259**: p. 113822.
33. Reza, M.S., et al., *Biochar characterization of invasive Pennisetum purpureum grass: effect of pyrolysis temperature.* Biochar, 2020. **2**(2): p. 239-251.

34. Wei, L., et al., *Biochar characteristics produced from rice husks and their sorption properties for the acetanilide herbicide metolachlor.* Environmental Science and Pollution Research, 2017. **24**(5): p. 4552-4561.
35. Liu, Y., Z. He, and M. Uchimiya, *Comparison of biochar formation from various agricultural by-products using FTIR spectroscopy.* Modern Applied Science, 2015. **9**(4): p. 246.
36. Chaves Fernandes, B.C., et al., *Impact of pyrolysis temperature on the properties of eucalyptus wood-derived biochar.* Materials, 2020. **13**(24): p. 5841.
37. Yang, T., et al., *Effect of pyrolysis temperature on the bioavailability of heavy metals in rice straw-derived biochar.* Environmental Science and Pollution Research, 2021. **28**(2): p. 2198-2208.
38. de Andrade, M.A., et al., *Combined Analytical Py-GC/MS, SEM, FTIR and 13 C NMR for Investigating the Removal of Trace Metals from Aqueous Solutions by Biochar.* Journal of the Brazilian Chemical Society, 2020. **31**: p. 1518-1530.
39. Domingues, R.R., et al., *Properties of biochar derived from wood and high-nutrient biomasses with the aim of agronomic and environmental benefits.* PloS one, 2017. **12**(5): p. e0176884.
40. Singh, B., M. Camps-Arbestain, and J. Lehmann, *Biochar: a guide to analytical methods*. 2017: Csiro Publishing.
41. Thommes, M. and K.A. Cychosz, *Physical adsorption characterization of nanoporous materials: progress and challenges.* Adsorption, 2014. **20**(2): p. 233-250.
42. Sahoo, S.S., et al., *Production and characterization of biochar produced from slow pyrolysis of pigeon pea stalk and bamboo.* Cleaner Engineering and Technology, 2021. **3**: p. 100101.
43. Ahmed, M.J., *Adsorption of quinolone, tetracycline, and penicillin antibiotics from aqueous solution using activated carbons.* Environmental toxicology and pharmacology, 2017. **50**: p. 1-10.
44. Dutta, S., et al., *Application of response surface methodology for preparation of low-cost adsorbent from citrus fruit peel and for removal of methylene blue.* Desalination, 2011. **275**(1-3): p. 26-36.
45. Li, F., et al., *Effects of biochars prepared from cassava dregs on sorption behavior of ciprofloxacin.* Procedia Environmental Sciences, 2016. **31**: p. 795-803.
46. Ahmed, M.B., et al., *Single and competitive sorption properties and mechanism of functionalized biochar for removing sulfonamide antibiotics from water.* Chemical Engineering Journal, 2017. **311**: p. 348-358.
47. Peiris, C., et al., *Biochar based removal of antibiotic sulfonamides and tetracyclines in aquatic environments: a critical review.* Bioresource Technology, 2017. **246**: p. 150-159.